

# Electronic structure of complex *spd* Hume-Rothery phases in transition-metal aluminides

Guy Trambly de Laissardière<sup>1</sup>, Duc Nguyen-Manh<sup>2</sup>, Didier Mayou<sup>3</sup>

<sup>1</sup> Laboratoire de Physique Théorique et Modélisation, CNRS / Université de Cergy–Pontoise, 95302 Cergy–Pontoise

<sup>2</sup> UKAEA Culham Division, Culham Science Centre, Abingdon, OX14 3DB, United Kingdom

<sup>3</sup> Laboratoire d’Etudes des Propriétés Electronique des Solides, CNRS, B.P. 166, 38042 Grenoble Cedex 9, France

Keywords: *spd* Hume-Rothery alloys, complex aluminides, quasicrystals, electronic structure

The discovery of quasicrystals phases and approximants in Al(rich)–Mn system has revived the interest for complex aluminides containing transition-metal atoms. On one hand, it is now accepted that the Hume-Rothery stabilization plays a crucial role. On the other hand, TM atoms have also a very important effect on their stability and their physical properties. In this paper, we review studies that unifies the classical Hume-Rothery stabilization for *sp* electron phases with the virtual bound state model for transition-metal atoms embedded in the aluminum matrix. These studies lead to a new theory for “*spd* electron phases”. It is applied successfully to Al(Si)–transition-metal alloys and it gives a coherent picture of their stability and physical properties. These works are based on first-principles calculations of the electronic structure and simplified models, compared to experimental results.

A more detailed review article is published in Prog. Mater. Sci. 50 (2005) p. 679-788.

## Contents

<b>1</b>	<b>Introduction</b>	<b>2</b>
<b>2</b>	<b>Density of states of <i>spd</i> electron phases</b>	<b>3</b>
2.1	Pseudogap . . . . .	4
2.2	<i>sp-d</i> hybridization . . . . .	4
2.3	Effect of the TM atom’s position . . . . .	6
2.4	Effective Mn–Mn interactions induce the pseudogap . . . . .	6
2.5	Negative valence of transition-metal atoms . . . . .	8
<b>3</b>	<b>Generalization of the Jones theory for the <i>spd</i> electron phases</b>	<b>10</b>
<b>4</b>	<b>Stability of complex <i>spd</i> electron phases</b>	<b>10</b>
4.1	Ab initio studies of the phase stability . . . . .	10
4.2	Effective TM–TM medium-range interactions stabilize Al–TM aluminides . . . . .	12

<b>5</b>	<b>Origin of the vacancy in hexagonal <math>\beta</math>-Al<sub>9</sub>Mn<sub>3</sub>Si and <math>\varphi</math>-Al<sub>10</sub>Mn<sub>3</sub></b>	<b>15</b>
5.1	ab initio study . . . . .	15
5.2	Medium-range Mn–Mn interaction can induce vacancies in the atomic structure	17
<b>6</b>	<b>Magnetism of Al(Si)–Mn phases</b>	<b>18</b>
6.1	Introduction and ab initio studies of magnetism . . . . .	18
6.2	The magnetic Mn–Mn effective interaction . . . . .	20
<b>7</b>	<b>Electronic localization</b>	<b>21</b>
7.1	Electronic transport . . . . .	21
7.2	Cluster virtual bound states . . . . .	23
7.3	Band-gap in some Al–TM alloys . . . . .	25
<b>8</b>	<b>Conclusion</b>	<b>26</b>
<b>9</b>	<b>Acknowledgements</b>	<b>27</b>

# 1 Introduction

Aluminides can form a large variety of atomic complex structures among them transition metal aluminides are of particular interest: they have potential applications due to their high strength and light weight. Some of these phases are quasicrystalline, thermodynamically stable, and present a very high structural quality and specific properties. At the same time their phase diagrams are complex and in particular that of Al–Mn is still incomplete. These are often structurally complex and bear resemblance with medium-range structure of quasicrystalline phases. All these facts raise fundamental questions concerning the electronic structure and the stability of transition-metal aluminides and also the occurrence of quasiperiodicity among these phases.

Very early, G. V. Raynor [1] has proposed to extend the Hume-Rothery concept [2, 3, 4] to *sp* alloys containing transition-metal atoms (TM atoms, TM = Ti, V, Cr, Mn, Fe, Co, and Ni). He showed that the rules for the appearance of crystalline structures as a function of an average number of valence electrons per atom  $e/a$  could be extended provided that a “*negative valence*” was given to transition metal atoms. He interpreted this as a negative charge that was located on the transition metal atom and a filled  $d$  band. This interpretation is not appropriate since it would correspond to a great electrostatic energy and indeed experiment show that it is not the case. Another difficulty with a too naive extension of the standard theory of Hume-Rothery phases concerns the experimental values of the density of states. The density presents a minimum at the Fermi energy (“*pseudogap*”) in most systems. Yet one expects that in a nearly-free electron gas the  $d$  orbitals of transition metal give a strong contribution to the total density of states in accordance with the Virtual Bound States model of the impurity limit (J. Friedel [5] and P.W. Anderson [6]). In this model there is only a very small transfer at the opposite of Raynor assumption. Thus, it appears that the role of transition metal atoms in aluminides is explained neither by the Raynor assumption, nor by the standard Virtual Bound States model. Now the Al(rich)–TM quasicrystals and related phases are often considered as Hume-Rothery alloys (see for instance [7, 8, 9, 10, 11]), but the problem of the physical interpretation of electronic structure of TM atoms still persists.

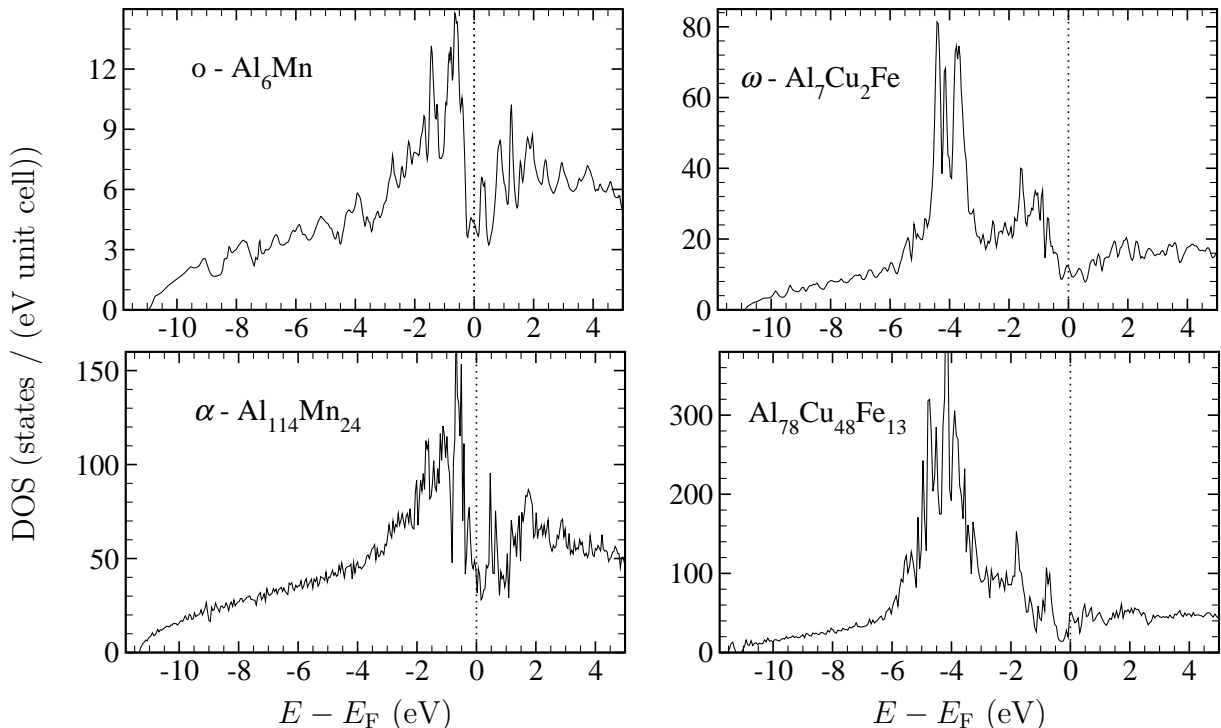


Figure 1: LMTO total DOS orthorhombic of  $o$ -Al<sub>6</sub>Mn, tetragonal  $\omega$ -Al<sub>7</sub>Cu<sub>2</sub>Fe, cubic  $\alpha$ -Al-Mn and cubic  $\alpha'$ -Al-Cu-Fe [13].

In this paper we summarize our work on the electronic structure of Al(rich)-TM phases that lead to consider these aluminides as “*spd Hume-Rothery compounds*”. Our study is based on numerous ab initio calculation on band structure calculations (using the self-consistent tight-binding Linear Muffin-Tin Orbital (LMTO) method [12]), and comparison with simple but physical Hamiltonian models. A more detailed review article is in preparation [13].

## 2 Density of states of *spd* electron phases

In the literature, there are a lot of theoretical studies of the electronic structure of Al(rich)-TM crystals and Al(rich)-TM crystalline approximants of quasicrystals from first-principles. In this section we focus on properties that are common to those phases in spite of different atomic structures. Some of these phases are rather “*simple*” phases that contain a small number of atoms in a unit cell, whereas other phases are “*complex*” phases that contain large number of atoms in a unit cell (table 1).

At low energy, the total DOS is nearly-free electrons like (figure 1). These states are mainly *sp* states of the Al atoms. The *d* states of TM (TM = Ti, V, Cr, Mn, Fe, Co, Ni) are observed in the middle of the *sp* band. In phases containing Cu atoms, the *d* peak of Cu is strong and it is located at an energy lower than that of *d* peak of TM.

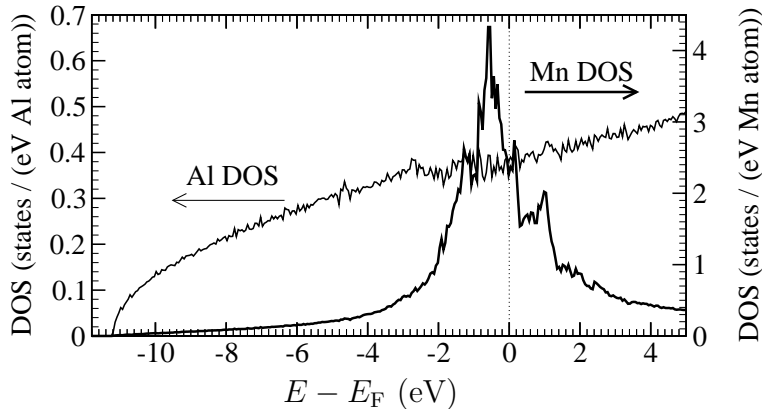


Figure 2: Non-magnetic DOS in a  $\text{Al}_{107}\text{Mn}$  model. Mn atoms are in substitution to Al atoms in an Al f.c.c. Al(1) and Mn atoms are first-neighbors.

## 2.1 Pseudogap

In many transition-metal aluminides, the Fermi level  $E_F$  is found near a large valley in the DOS that splits the band between bonding states and anti-bonding states (figure 1). This valley, called “*pseudogap*”, is generally attributed to a combined effect including the electron diffraction by the Bragg planes of a prominent Brillouin zone and a strong Al(*sp*)–TM(*d*) hybridization [14, 15] (see following section). As shown in table 1, this pseudogap is predicted from first-principles in the Al DOS (mainly *sp* DOS) of most of the simple phases and the complex phases (see Refs. in [13]). It is also predicted in the total DOS and the TM DOS (mainly *d* states) of many phases ( $\alpha$ - $\text{Al}_6\text{Mn}$ ,  $\alpha$ - $\text{Al-Mn-Si}$ , ...) (figure 3). But in the phases containing a concentration of Mn atoms larger than 20 %, the pseudogap can be filled (or partially filled) by the *d* states of some TM atoms (T-Al-Pd-Mn,  $\text{Al}_3\text{Mn}$ , ...) (figure 4). Photo-emission spectroscopy and specific heat measurements [17] have confirmed the presence of pseudogap in the DOS of many Al–TM quasicrystals and approximants.

## 2.2 *sp-d* hybridization

The *spd* aluminides are characterized by a strong *sp-d* hybridization between the Al *sp* states and the TM *d* orbitals. Many experimental studies of photoemission spectra have shown this property (E. Belin-Ferré in this proceedings). It is illustrated from LMTO calculation by the comparison between the DOSs calculated with the *sp-d* hybridization (“exact” calculation) and the DOSs calculated by setting to zero the matrix elements of the Hamiltonian that correspond to the *sp-d* hybridization (calculation “without *sp-d* hybridization” [19]) (figure 3). The width of the TM DOS is strongly reduced in the calculation without *sp-d* hybridization with respect to the exact calculation. Indeed the width of the TM DOS (mainly *d* DOS) is proportional to the square of the matrix element that couples the *d* states and the *sp* states in the Hamiltonian

In the case of a TM impurity in the free electron matrix (Virtual Bound States model) [5, 6], the partial *d* DOS is a Lorentzian and the free states *sp* DOS is not modified by the *sp-d* hybridization (compensation theorem). This is illustrated by the LMTO calculation (without spins polarization) for Mn diluted in the Al f.c.c. crystals (figure 2). We have considered a super-cell of Al structure containing 108 atoms. An Mn substitutes one of the Al atoms in the super-cell, thus as the concentration is  $\text{Al}_{107}\text{Mn}$ .

Table 1: Examples of Al–Mn crystals.

$\mathcal{N}$  is the number of atoms per unit cell. Calculated DOS at the energy  $E_{min}$  for which the total DOS reaches its minimum in the pseudogap:  $n$ , total DOS (states/eV atom);  $n_{Al}$ , local Al DOS (states/eV Al atom);  $n_{Mn}$ , local Mn DOS (states/eV Mn atom).

References of the crystallographic structures are given in Ref. [13]

Phase	Space group	$\mathcal{N}$	% Mn atoms	LMTO DOS at $E_{min}$			
				$n$	$n_{Al}$	$n_{Mn}$	Refs.
Al	cubic f.c.c.	1	0	0.30	0.30	–	[15]
Al <sub>107</sub> Mn †	cubic	108	0.9	0.36	0.34	2.60	[13]
Al <sub>31</sub> Mn †	cubic	32	3.1	0.37	0.33	1.78	[13]
Al <sub>12</sub> Mn	cubic Im3	13	7.7	0.22	0.18	0.69	[15]
o-Al <sub>6</sub> Mn	orthorhombic Cmcm	14	14.3	0.20	0.11	0.75	[15]
Al <sub>65.9</sub> Pd <sub>12.2</sub> Mn <sub>14.6</sub> Si <sub>7.3</sub>	Cubic Pm3	123	14.6	0.12	0.06	0.45	[39]
T-Al <sub>79.5</sub> Pd <sub>5.1</sub> Mn <sub>15.4</sub>	orthorhombic Pnma	156	15.4	0.21	0.10	0.79	[39]
$\alpha$ -Al <sub>114</sub> Mn <sub>24</sub>	cubic Pm $\bar{3}$	138	17.4	0.21	0.13	0.58	[8, 50]
$\mu$ -Al <sub>4.12</sub> Mn	hexagonal P6 <sub>3</sub> /mmc	568	19.4	0.38*	0.15*	1.32*	[16, 13]
$\varphi$ -Al <sub>10</sub> Mn <sub>3</sub>	hexagonal P6 <sub>3</sub> /mmc	26	23.1	0.16	0.07	0.47	[38]
Al <sub>13</sub> Mn <sub>4</sub> ‡	monoclinic C2/m	51	23.6	0.22	0.10	0.60	[13]
T-Al <sub>3</sub> Mn	orthorhombic Pnma	156	30.8	0.29	0.10	0.71	[46, 13]

† Hypothetical model for an Mn impurity in the Al matrix: Mn substituted Al in the Al f.c.c. lattice

‡ Structure of Al<sub>13</sub>Fe<sub>4</sub> [18].

\* Preliminary results.

In Al–TM phases the  $sp$ – $d$  hybridization is strong too, but the Virtual Bound States model is no more valid. Indeed, many theoretical and experimental studies shows that  $sp$ – $d$  hybridization plays a crucial role in the pseudogap formation. In some cases (Al<sub>3</sub>Ti, o-Al<sub>6</sub>Mn,  $\omega$ -Al<sub>7</sub>Cu<sub>2</sub>Fe,  $\alpha$ -Al–Mn, ...) the pseudogap is present in the calculation without  $sp$ – $d$  hybridization and it is increased by the  $sp$ – $d$  hybridization (figure 3). In other cases ( $\beta$ -Al<sub>9</sub>Mn<sub>3</sub>Si,  $\varphi$ -Al<sub>10</sub>Mn<sub>3</sub>, ...) the pseudogap disappears when  $sp$ – $d$  hybridization is suppressed [38].

Let’s remark that in some particular cases the direct  $d$ – $d$  coupling between two first-neighbors TM could be important. But in many Al(rich)–TM alloys (Al<sub>3</sub>Ti, o-Al<sub>6</sub>Mn,  $\omega$ -Al<sub>7</sub>Cu<sub>2</sub>Fe,  $\alpha$ -Al–Mn, ...) TM atoms are not first-neighbors, therefore the direct  $d$ – $d$  coupling is not enough to explain the generic properties of the Al–TM DOS.

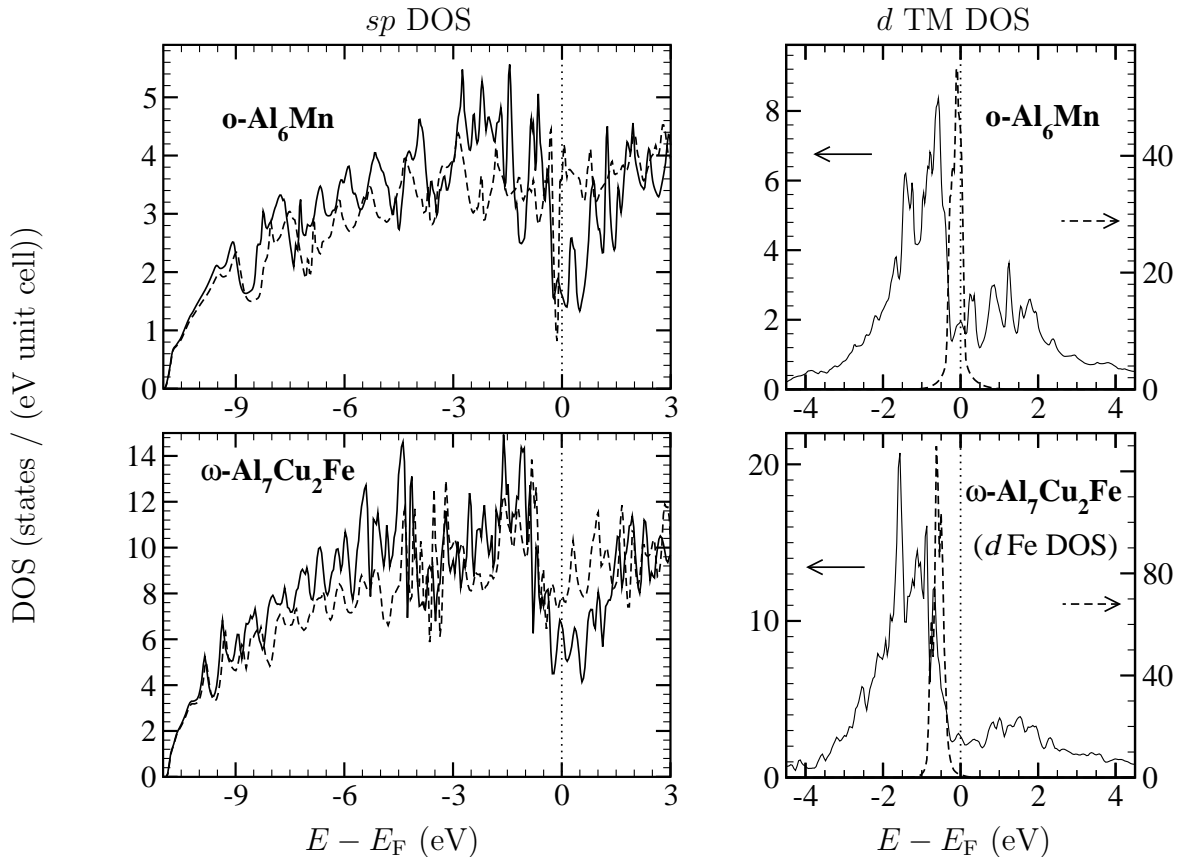


Figure 3: LMT0  $sp$  Al DOS and  $d$  TM DOS of crystals. Solid lines, exact calculation; dashed lines, calculations without  $sp$ - $d$  hybridization. [15]

### 2.3 Effect of the TM atom's position

In the Virtual Bound State model [5, 6], the  $sp$  free states have a uniform amplitude in the real space, thus the  $d$  TM DOS does not depend on the position,  $\mathbf{r}_{TM}$ , of the TM atom. But, in Hume-Rothery phases, the diffraction by Bragg planes is important ( $sp$  states are not free states) and the amplitude of  $sp$  states depends on  $\mathbf{r}$ . Therefore, the effect of the  $sp$ - $d$  coupling on the DOSs depends on  $\mathbf{r}_{TM}$ . In the literature there are many examples of ab initio calculations showing different local TM DOSs of inequivalent TM sites. In the case of the orthorhombic T-Al-Pd-Mn (figure 4), Mn(2) and Mn(5) local DOSs have a pseudogap near  $E_F$ , whereas Mn(3) and Mn(4) local DOSs do not have.

We have developed a model to calculate the TM DOS in Al-TM phase which takes into account the diffraction of the  $sp$  states by the Bragg planes of a prominent Brillouin zone [14, 15, 13]. The TM position is a crucial parameter that can switch on or switch off the pseudogap in the local DOS around TM.

### 2.4 Effective Mn-Mn interactions induce the pseudogap

Considering that the pseudopotential of Al atoms is small, Al(rich)-TM phases are modeled by a collection of TM atoms in a jellium (free electron states of Al). The total DOS,  $n$ , is written as:

$$n(E) = n_{\text{free}}(E) + \Delta n_{\text{TM}s}(E), \quad (1)$$

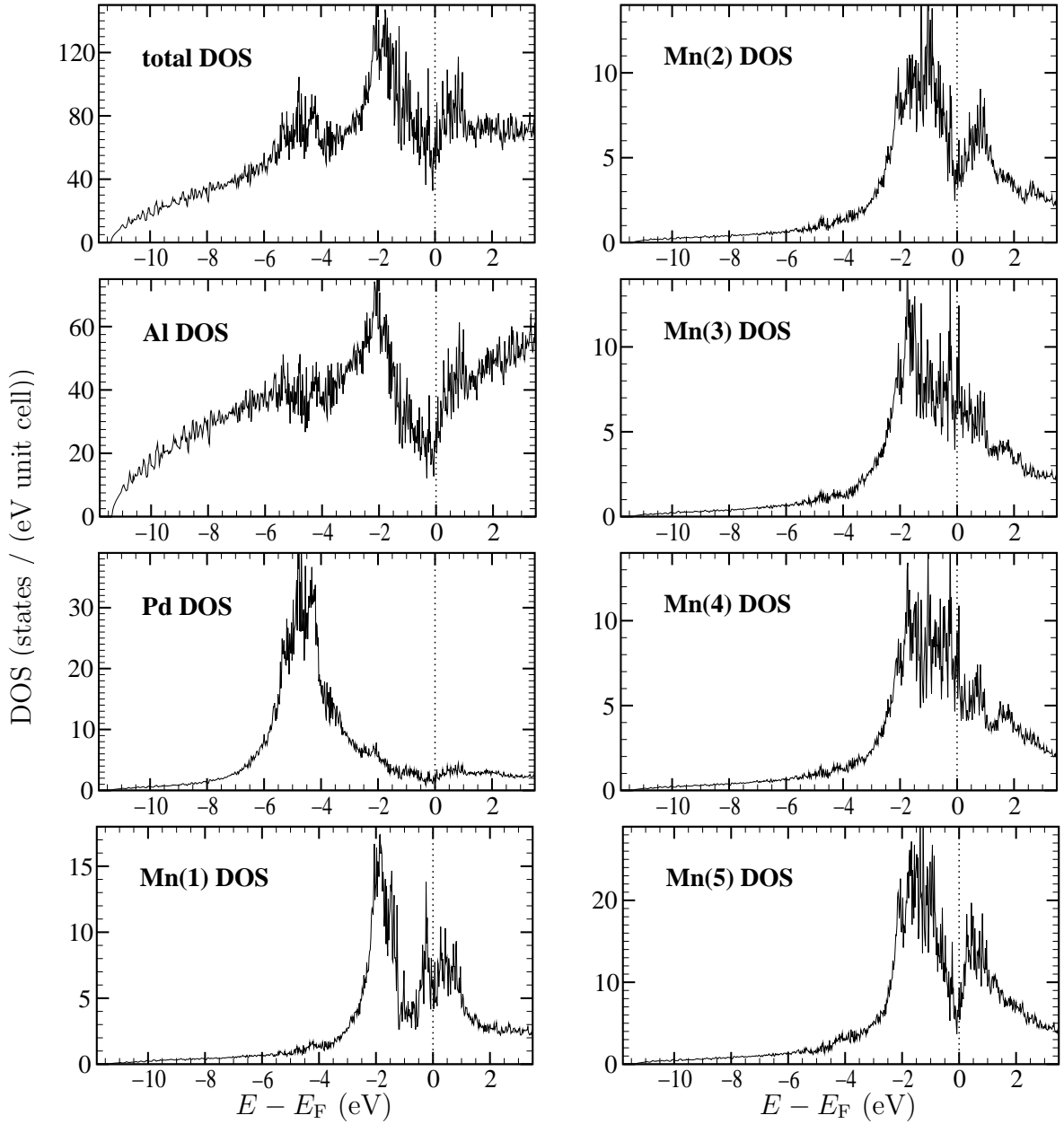


Figure 4: LMTO total DOS and local DOSs of the orthorhombic T-Al<sub>79.5</sub>Pd<sub>5.1</sub>Mn<sub>15.4</sub> phase, calculated without spin polarization [39].

where,  $n_{\text{free}}$  is the DOS of free  $sp$  states, and  $\Delta n_{\text{TM}s}$  the variation of the total DOS due to the TM atoms. We calculated  $\Delta n_{\text{TM}s}$  as the sum of variation of the DOS due to each Mn-Mn pair [21]. When all the TM atoms are on the same Wyckoff position,  $\Delta n_{\text{TM}s}$  per TM atoms is:

$$\Delta n_{\text{TM}s}(E) = \Delta n_{1\text{TM}}(E) + \frac{1}{2} \sum_{j \neq 1} \left( \Delta n_{2\text{TM}}(E, r_{1j}) - 2\Delta n_{1\text{TM}}(E) \right), \quad (2)$$

where  $j$  is an index the TM atoms.  $\Delta n_{1\text{TM}}$  is the variation of the DOS due to one TM impurity in free electron (Lorentzian, i.e. Virtual Bound State), and  $\Delta n_{2\text{TM}}$ , the variation of the DOS due to two TM atoms in free electrons calculated by the Lloyd formula (using

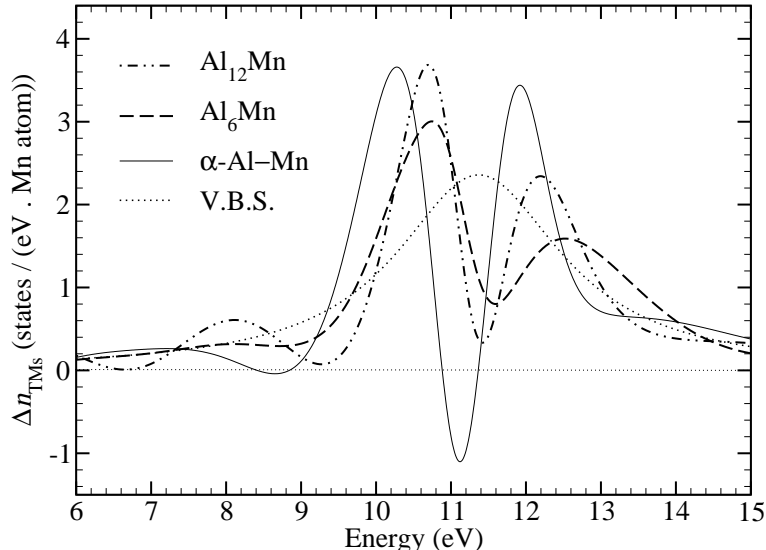


Figure 5: Variation of the DOS,  $\Delta n_{\text{TM}_s}$  due to the Mn sub-lattice, in  $\text{Al}_{12}\text{Mn}$ ,  $\text{o-Al}_6\text{Mn}$ , and  $\alpha\text{-Al-Mn}$ . V.B.S. is the case of one Mn impurity in the Al matrix (Virtual Bound State). [21]

transfer matrix  $\mathbf{T}$  approach) [22]. We have calculated  $\Delta n_{\text{Mn}}$  for Al-Mn phases where Mn atoms are not first-neighbors:  $\text{Al}_{12}\text{Mn}$ ,  $\text{o-Al}_6\text{Mn}$ , and  $\alpha\text{-Al-Mn}$ . The sum in (2) is computed including the distances  $r_{1j}$  up to the distance  $R$ . A well pronounced pseudogap appears when  $r_{1j}$  up to 10–20 Å are taken into account [21]. Results with  $R = 15$  Å are presented in figure 5. For  $\alpha\text{-Al-Mn}$  structure, negative values of  $\Delta n_{\text{Mn}}$  are obtained for some energy, which induces a reduction of the total DOS with respect to the free electrons DOS,  $n_{\text{free}}(E)$ , at these energies (equation (1)). These results show that effective medium-range Mn-Mn interaction contribute to the pseudogap in those Al(rich)-TM phases.

## 2.5 Negative valence of transition-metal atoms

In his original work on negative valence Raynor [1] assumed a transfer of electrons from the conduction band ( $sp$  band) to the  $d$  band in order to compensate the unpaired spins of the TM elements, and fill the  $d$  band. In this scheme the TM atoms remove electrons from the  $sp$  band and thus have a negative valence. But a transfer of several electrons on one atom is unrealistic in metallic alloys since it corresponds to a too large electrostatic energy for metallic alloys [2].

The LMTO results allow to solve this paradox and to understand the apparent negative valence of TM in Al-TM compounds. Indeed, there is an increase of the  $sp$  DOS below  $E_{\text{F}}$  as compared to the free electron DOS due to the combined effect of  $sp-d$  hybridization and the diffraction of  $sp$  states by Bragg planes. In this scheme filling these additional  $sp$  states below  $E_{\text{F}}$  plays the same role as filling of the  $d$  band in Raynor’s scheme. It results in an apparent negative valence of TM. Contrary to the  $d$  orbitals these additional  $sp$  states are delocalized and do not lead to a strong electrostatic energy. Yet one may expect that these additional  $sp$  states are linked to the TM atom and that they follow its displacement. This could explain the anomalous effective charge of TM elements as deduced from optical conductivity [24].



Table 2: Negative valence of transition-metal elements in Al(rich) alloys:  
According to Raynor [1] and quantity ( $-\Delta N_{sp}$ ) calculated from LMTO [14].

	Cr	Mn	Fe	Co	Ni
Raynor	-4.66	-3.66	-2.66	-1.66	-0.66
LMTO	-3.2 (Al <sub>12</sub> Cr)	-2.7 (Al <sub>12</sub> Mn) -2.0 (Al <sub>6</sub> Mn)	-2.5 (Al <sub>7</sub> Cu <sub>2</sub> Fe)	-1.3 (Al <sub>9</sub> Co <sub>2</sub> ) -0.9 (Al <sub>5</sub> Co <sub>2</sub> )	-1 (Al <sub>3</sub> Ni)

The variation of the number  $d$  of electrons and  $sp$  electrons due to the TM impurity are, respectively,

$$N_d = \int^{E_F} n_d(\epsilon) d\epsilon \quad \text{and} \quad \Delta N_{sp} = \int^{E_F} \Delta n_{sp}(\epsilon) d\epsilon. \quad (3)$$

$N_d$  is fixed by the nature of the TM atom.  $\Delta N_{sp}$  is the variation of  $sp$  electrons due to the presence of the TM atoms. When  $sp$  states are free (no diffraction by Bragg planes),  $\Delta N_{sp} = 0$ , but in actual Al(rich)-TM alloys,  $sp$  states are not free and  $\Delta N_{sp}$  takes a positive value. From LMTO it can be estimated as (table 2):

$$\Delta N_{sp} = N_{sp} - N_{sp}(\text{without } sp-d \text{ hybridization}), \quad (4)$$

The quantity

$$\mathcal{A} = -\Delta N_{sp}, \quad (5)$$

given per TM atom, is what Raynor called a negative valence of TM. It corresponds to an increase of the  $sp$  electrons density around the TM impurity, but it is not a charge transfer from  $sp$  band to  $d$  orbitals. Note that this apparent negative valence depends on the nature of TM element but also on the Al-TM compounds. Indeed as seen in the first section the local TM DOS depends on the position of the TM atom in the crystals.

The origin of the additional  $sp$  electrons is understandable from a simple argument based on a sum rule. Consider first the limiting case for which the diffraction by Bragg plans creates a gap in the DOS at  $E_F$ . Consider also 5 degenerated  $d$  orbitals of a non-magnetic TM impurity in the the free electron matrix (jellium). When  $E_d \ll E_F$ , it is obvious that

$$N_d + \Delta N_{sp} = 10 \text{ electrons}, \quad (6)$$

since the  $d$  band is filled and  $\Delta N_{sp} = 0$ . If  $E_d$  is shifted continuously up a realistic value close to  $E_F$  the eigen energies should be shifting continuously too. Thus, no states could jump the gap and the total number of states below  $E_F$  is independent of the value of  $E_d$  (when  $E_d \leq E_F$ ). Therefore, if there is a gap a  $E_F$ , the equation (6) is always satisfied for  $E_d \leq E_F$ , and one obtains that

$$\mathcal{A} = -(10 - N_d) < 0. \quad (7)$$

In actual alloys where there is a pseudogap at  $E_F$  (not a gap), one could conjecture that the equality in (7) becomes an inequality:

$$-(10 - N_d) < \mathcal{A} < 0, \quad (8)$$

with an apparent valence of TM still negative.

### 3 Generalization of the Jones theory for the *spd* electron phases

For *sp* Hume-Rothery alloys, the valence states (*sp* states) are nearly-free states scattered by a weak Bragg potential,  $V_B$  (Jones theory, see Refs. [3, 4]). But, the treatment of Al(rich) alloys containing TM atoms requires a different model because the *d* states of TM are not nearly-free states [14, 15]. In this section, we show briefly that in *spd* Hume-Rothery alloys, the *sp* electrons feel an “*effective Bragg potential*” [15] that takes into account the strong effect TM atoms via the *sp-d* hybridization.

Following a classical approximation [5, 6] for Al(Si)-Mn alloys, a simplified model is considered where *sp* states are nearly-free and *d* states are localized on Mn sites  $i$ . The effective Hamiltonian for the *sp* states is written:

$$H_{eff(sp)} = \frac{\hbar^2 k^2}{2m} + V_{B,eff} \quad (9)$$

where  $V_{B,eff}$  is an effective Bragg potential that takes into account the scattering of *sp* states by the strong potential of Mn atoms.  $V_{B,eff}$  depends thus on the positions  $\mathbf{r}_i$  of Mn atoms. Assuming that all Mn atoms are equivalent and that two Mn atoms are not first-neighbor, one obtains:

$$V_{B,eff}(\mathbf{r}) = \sum_{\mathbf{K}} V_{B,eff}(\mathbf{K}) e^{i\mathbf{K}\cdot\mathbf{r}}, \quad (10)$$

$$V_{B,eff}(\mathbf{K}) = V_B(\mathbf{K}) + \frac{|t_{\mathbf{K}}|^2}{E - E_d} \sum_i e^{-i\mathbf{K}\cdot\mathbf{r}_i}, \quad (11)$$

where the vectors  $\mathbf{K}$  belong to the reciprocal lattice,  $t_{\mathbf{K}}$  is a average matrix element that couples *sp* states  $\mathbf{k}$  and  $\mathbf{k} - \mathbf{K}$  via the *sp-d* hybridization, and  $E_d$  is the energy of *d* states. The term  $V_B(\mathbf{K})$  is a weak potential independent of the energy  $E$ . It corresponds to the Bragg potential for *sp* Hume-Rothery compounds.

The last term in equation (11), is due to the *d*-resonance of the wave function by the potential of Mn atoms. It is strong in an energy range  $E_d - \Gamma \leq E \leq E_d + \Gamma$ , where  $2\Gamma$  is the width of the *d* DOS. This term is essential as it does represent the diffraction of the *sp* electrons by a network of *d* orbitals, i.e. the factor  $(\sum_i e^{-i\mathbf{K}\cdot\mathbf{r}_i})$  corresponding to the structure factor of the TM atoms sub-lattice. As the *d* band of Mn is almost half filled,  $E_F \simeq E_d$ , this factor is important for energy close to  $E_F$ . Note that the Bragg planes associated with the second term of equation (11) correspond to Bragg planes determined by diffraction.

This qualitative analysis suggests that both *sp-d* hybridization and diffraction of *sp* states by the sub-lattice of Mn atoms are essential to understand the electronic structure of Al(Si)-Mn alloys. The strong effect of *sp-d* hybridization on the pseudogap is then understood in the framework of Hume-Rothery mechanism.

## 4 Stability of complex *spd* electron phases

### 4.1 Ab initio studies of the phase stability

First-principles electronic structure calculations have proven to be an accurate and efficient tool to understand the physics of materials in particular in investigating systematically

the energetics and (meta)stability of transition-metal aluminides alloys [25, 26, 27, 28]. Although there have been several first-principles calculations for different Al(rich)–TM compounds and related quasicrystalline phases, it is desirable to elucidate why the quasicrystalline phase is stable only by forming with *TM* of group VIIA (Mn, Re) and group VIIIA (Fe, Ru, Os, Co, Rh, Ir, Ni)? It is also essential to know whether these calculations confirm (or not) a Hume-Rothery mechanism for stabilizing *spd* compounds like that has been shown for simple *sp* compounds.

In order to analyze the trend in structural stability of the transition-metal trialuminides across the transition metal series, the relative stability between the simple tetragonal  $I4/mmm$   $Al_3TM$  ( $Al_3V$  structure) and the complex monoclinic  $C2/m$   $Al_{13}TM_4$  ( $Al_{13}Fe_4$  structure) has been investigated using first-principles total energy and electronic structure calculations within the LMTO method [18].  $Al_3TM$  has a similar composition than  $Al_{13}TM_4$ , but a simpler tetragonal structure.

Considering first the case  $TM = Ru$ , from an ab initio calculated equilibrium volume, the heat of formation has been determined, and it is shown that monoclinic  $Al_{13}Ru_4$  is indeed more stable than  $Al_3Ru$  [18], as reported in Al-Ru binary phase diagram [20]. Moreover, a detailed investigation of the link between the density of states and the stability using ab initio calculations and a “frozen-potential” approach, shows the importance of the position of  $E_F$  [18]. Indeed,  $E_F$  is located near a peak in the DOS of  $Al_3Ru$ , whereas it is located in a the pseudogap in the DOS of  $Al_{13}Ru_4$  [18]. In the former structure, the central peak which is predominantly the “*non-bonding*” Ru *4d*, disappears from the DOS of  $Al_{13}Ru_4$  where there are now only bonding and anti-bonding hybrid *sp*(Al) and *d*(Ru) states between the nearest neighbors.

We have analyzed the non-bonding peak in Al-*TM* alloys across the transition-metal *3d* series using a model taking into account the diffraction by the Bragg plane in *spd* compounds [14, 15]. In the figure 6, the LMTO DOS of tetragonal  $Al_3TM$  and monoclinic  $Al_{13}TM_4$  are compared for  $TM = V, Mn$  and  $Fe$ . With Mn and Fe the results are similar to those with Ru [18], whereas the situation is the opposite with V. Indeed a non-bonding peak is observed in the DOS of monoclinic  $Al_{13}V_4$  whereas  $E_F$  is near the pseudogap in the DOS of tetragonal  $Al_3V$ .

By using a Rigid Band Approximation within local Density Functional theory, the effect of the number of electrons per atom  $e/a$  on the relative stability has been studied [18]. This shows (figure 7) that transition-metal trialuminides goes from the tetragonal  $Al_3TM$  structure to the monoclinic  $Al_{13}TM_4$  structure as a function of the electron per atom ratio. The  $Al_3TM$  structure is more stable for transition-metal trialuminides with *TM* at the beginning of the *d* series (Sc, Ti, V, Y, Zr, Nb, La, Hf, Ta) whereas  $Al_{13}Fe_4$  structure is more stable for transition-metal trialuminides with  $TM = Mn, Fe, Co, Ni, Tc, Ru, Rh, Pd, Re, Os, Ir$  and  $Pt$  [18].

These theoretical predictions of the relative stability of the transition-metal trialuminides between the simple tetragonal  $Al_3TM$  structure and the more complex monoclinic  $Al_{13}TM_4$  structure, agrees with the Hume-Rothery condition for stabilization. Concerning the DOS, it results that the consequences of the Hume-Rothery rules are the same as for *sp* electron compounds: The most stable phases are those for which  $E_F$  is located in a pseudogap of the total DOS.

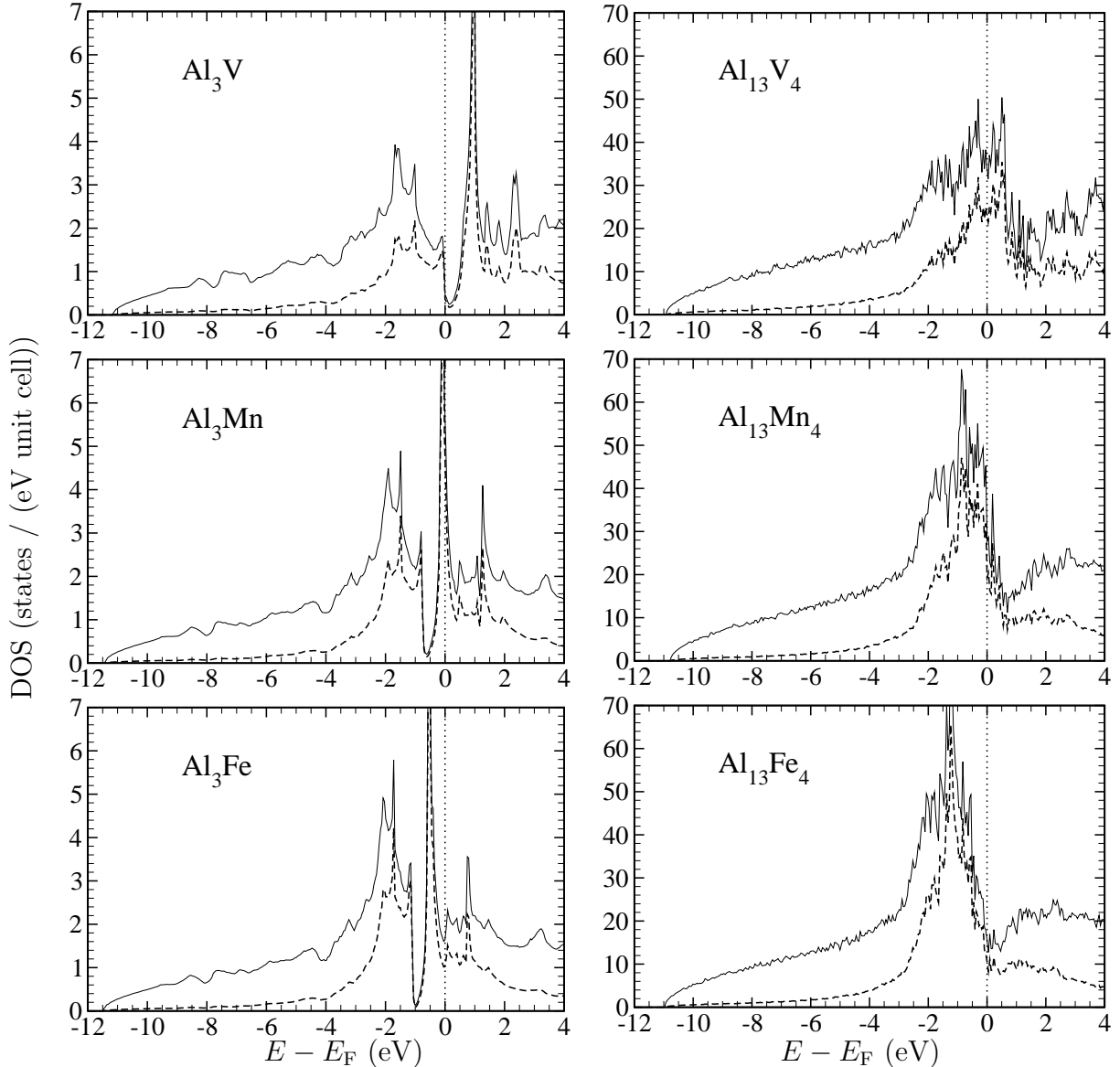


Figure 6: LMTO (line) total DOSs and (dashed line) TM DOSs of tetragonal  $I4/mmm$   $Al_3TM$  (structure and atomic positions of  $Al_3V$ ); and monoclinic  $C2/m$   $Al_{13}TM_4$  (structure and atomic positions of  $Al_{13}Fe_4$ ) for  $TM = V, Fe, Mn$ . [13]

## 4.2 Effective TM–TM medium-range interactions stabilize Al–TM aluminides

Zou and Carlsson [29] remarked first that in many Al–Mn crystals approximants and quasicrystals the Mn–Mn pair distances correspond to local minima of  $\Phi_{Mn-Mn}(r)$  up to 10 Å and more. That suggests the importance of the effective interaction over medium-range order for the stabilization of complex structure in Al(rich)–Mn phase diagram.

The internal energy  $U$  is calculated of all TM atoms in Al(Si) host. The reference energy,  $U = 0$ , is those of one TM in the Al matrix (TM impurity). It corresponds to the energy for the system where TM atoms are in the Al(Si) host and all TM–TM distances are equal to infinity. So,  $U$  is defined as the energy needed to built the structure from isolated

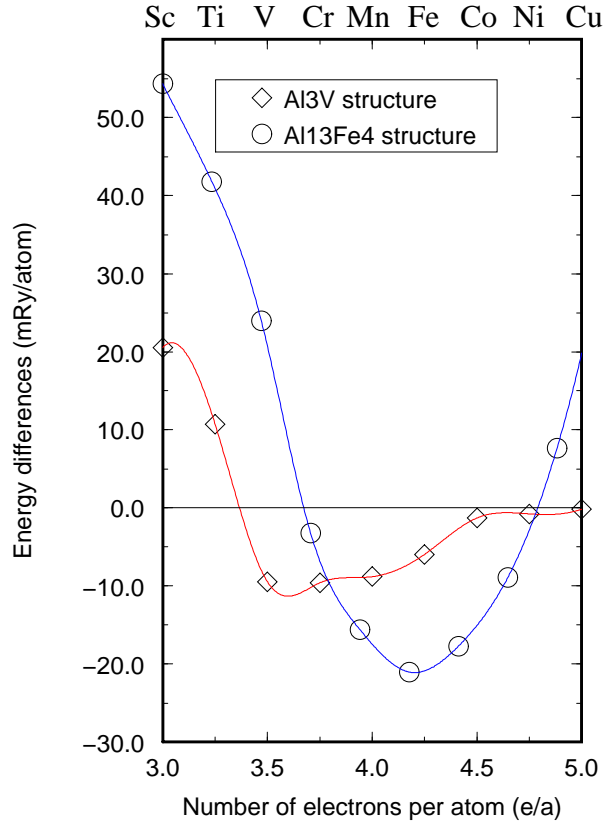


Figure 7: Structural energy difference between the tetragonal  $\text{Al}_3\text{TM}$  (I4/mmm  $\text{Al}_3\text{V}$  structure) and the monoclinic  $\text{Al}_{13}\text{TM}_4$  (C2/m  $\text{Al}_{13}\text{Fe}_4$  structure). [18]

TM atoms in the Al(Si) host. It appears as a “structural energy” of TM sub-lattice. For a crystal,  $U_{\text{TM}}$  per TM atom is:

$$U_{\text{TM}} = \frac{1}{\mathcal{N}_{\text{TM}}} \sum_{\text{TM}(k)} \alpha_k U_{\text{TM}(k)} , \quad (12)$$

The sum is on non-equivalent TM(k) Wyckoff sites.  $\alpha_k$  is the number of TM(k) atoms in a unit cell, and  $\mathcal{N}_{\text{TM}}$ ,  $\mathcal{N}_{\text{TM}} = \sum_k \alpha_k$ , the number of TM atoms in a unit cell.  $U_{\text{TM}(k)}$  is the part of the structural energy due to each TM(k) atom.  $U_{\text{TM}(k)}$  is computed from the TM–TM pair interaction:

$$U_{\text{TM}(k)} = \frac{1}{2} \sum_{i \neq k} \Phi_{\text{TM-TM}}(r_{ki}) e^{-\frac{r_{ki}}{L}} . \quad (13)$$

$r_{ki}$  is the distance between an atom  $\text{TM}_k$  (on TM(k) Wyckoff site) and  $\text{TM}_i$  atoms. The sum is over all  $\text{TM}_i$  atoms ( $\text{TM}_i \neq \text{TM}_k$ ).  $U_{\text{TM}(k)}$  takes the different values for all TM atom located on the different Wyckoff sites. The effective TM–TM interaction  $\Phi_{\text{TM-TM}}$  is calculated from the DOS of two TM in the Al matrix [13].  $L$  is mean-free path due to static disorder or/and by phonons [13]. It is difficult to estimate and depends on the structural quality and temperature. For metallic crystals and for approximants of quasicrystals, it should be larger than  $10 \text{ \AA}$  [13].

In  $\alpha\text{-Al}_6\text{Mn}$ ,  $\text{Al}_{12}\text{Mn}$  crystals and  $\alpha\text{-Al-Mn-Si}$  approximant, there is only one Mn Wyck-off position therefore  $U = U_{\text{Mn}}$ . In these phases there is no Mn first-neighbors. For phases

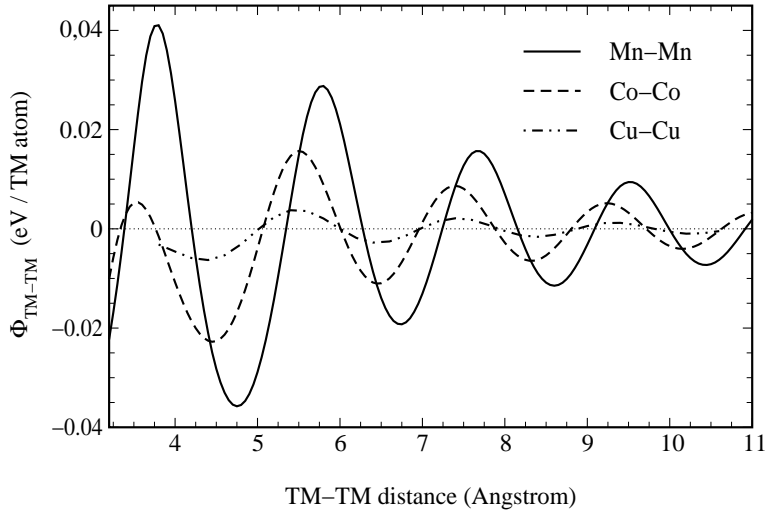


Figure 8: Effective medium-range pair interactions between two TM atoms in a jellium (free states) simulating the Al matrix.

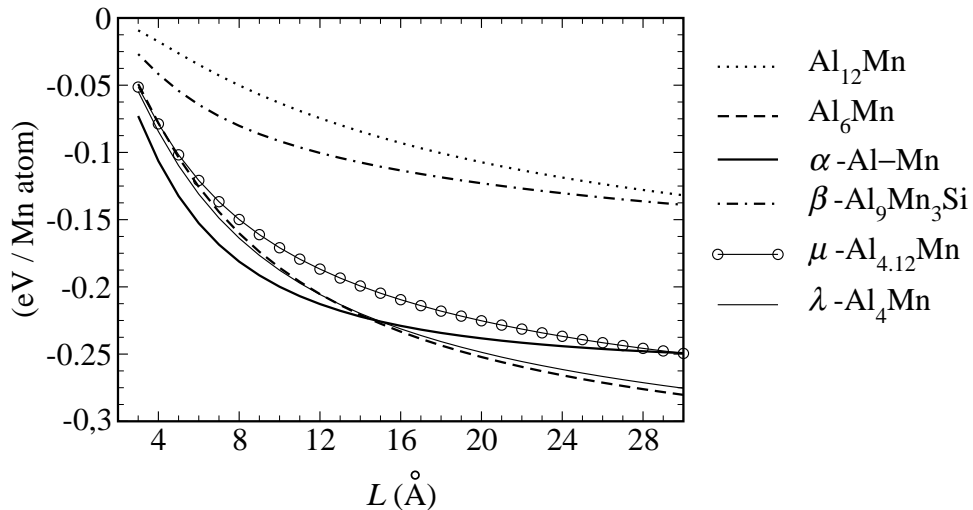


Figure 9: Structural energy the Mn sub-lattice of Al-Mn crystals. The first-neighbors Mn-Mn contributions are not include in the calculations. [13]

that contain first-neighbor Mn pairs, an energy  $U'_{TM(i)}$  is calculated without including the first-neighbor TM-TM terms in the sum (13). The corresponding  $U'$  is the part of the structural energy of TM sub-lattice that comes only from effective medium-range TM-TM interactions. For complex phases  $\mu$ -Al<sub>4.12</sub>Mn,  $\lambda$ -Al<sub>4</sub>Mn and Al<sub>3</sub>Mn,  $U'_{Mn(i)}$  for different Wyck-off Mn sites have qualitatively the same behavior; thus, we present their average structural energy of the Mn sub-lattice  $U' = \langle U'_{Mn(i)} \rangle_i$ . Figure 9 shows that the structural energy of the Mn sub-lattice is always negative, therefore the Mn-Mn interactions over medium-range distances contribute to stabilize these phases.

In the liquid the loss of the medium-range order and the small value of  $L$  lead to  $U$  close to zero. But it is still negative [30], in agreement with the fact that short-range and medium-range order do not disappeared completely [31, 32].

This approach is consistent with a Hume-Rothery stabilization. Indeed, the Hume-

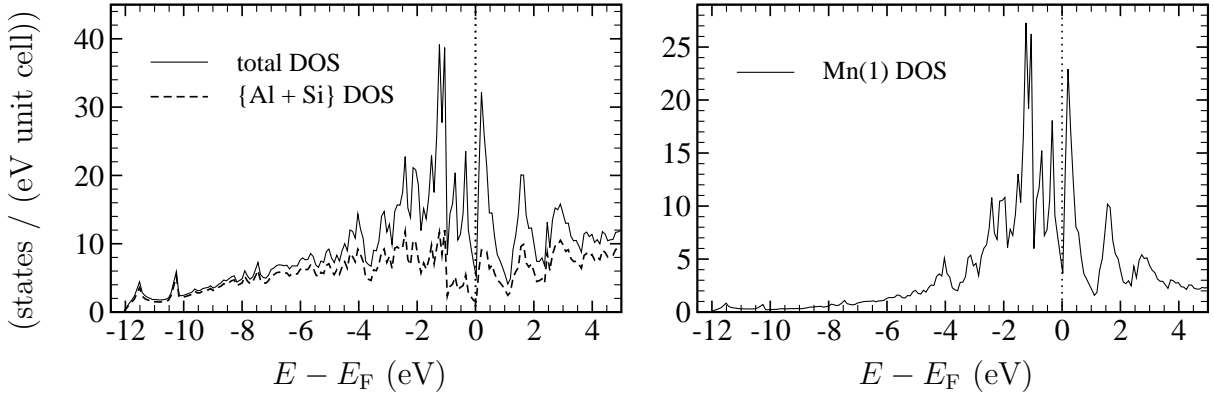


Figure 10: LMTO of hexagonal  $\beta$ - $\text{Al}_9\text{Mn}_3\text{Si}$ . [38]

Rothery mechanism can be expressed in terms of atomic interaction in the real space [33, 34].

## 5 Origin of the vacancy in hexagonal $\beta$ - $\text{Al}_9\text{Mn}_3\text{Si}$ and $\varphi$ - $\text{Al}_{10}\text{Mn}_3$

Interesting examples of Al–TM crystals, are given by the almost isomorphic stable  $\beta$ - $\text{Al}_9\text{Mn}_3\text{Si}$ , meta-stable  $\varphi$ - $\text{Al}_{10}\text{Mn}_3$  and stable  $\text{Al}_5\text{Co}_2$  phases. In 1952, Robinson suggested that these compounds with similar structure could be understood as Hume–Rothery phases with similar  $e/a$  ratios in spite of different atomic concentrations [35]. Indeed, a band energy minimization occurs when the Fermi sphere touches a pseudo-Brillouin zone, spanned by Bragg vectors  $\mathbf{K}_p$  corresponding to intense peaks in the experimental diffraction pattern.

In an hexagonal unit cell (P6<sub>3</sub>/mmc),  $\beta$ - $\text{Al}_9\text{Mn}_3\text{Si}$  ( $\varphi$ - $\text{Al}_{10}\text{Mn}_3$ ) contains 18 (20) Al, 2 (0) Si, and 6 (6) equivalent Mn (Mn(1) on Wyckoff site (6h)); and  $\text{Al}_5\text{Co}_2$  contains 20 Al, and 8 Mn (6 Co(1) on site (6h), and 2 Co(0) on site (2d)). A particularity of the atomic structure of  $\beta$  and  $\varphi$  phases is the presence of a large vacancy Va on site (2d). But in  $\text{Al}_5\text{Co}_2$ , this site is occupied by Co(0). This explains the difference of stoichiometry. It is thus interesting to understand why this vacancy is maintained in  $\beta$  and  $\varphi$  crystals? Because the first-neighbor distances around Va in  $\beta$ ,  $\varphi$  are close to those around Mn(1) in  $\beta$ ,  $\varphi$  and to those around Co in  $\text{Al}_5\text{Co}_2$ , the presence of Va cannot be explained from steric encumbering. Indeed, the environment of the vacancy in  $\beta$ ,  $\varphi$  forms a tri-capped trigonal prism (3 Al(1) and 6 Al(2)). A similar environment, with similar inter-atomic distances, is found in  $\mu$ - $\text{Al}_{4.12}\text{Mn}$  (Ref. [36]) and  $\lambda$ - $\text{Al}_4\text{Mn}$  (Ref. [37]). But in  $\mu$  and  $\lambda$ , these sites are occupied by Mn.

### 5.1 ab initio study

The LMTO total DOS and the local {Al + Si} DOS of  $\beta$ - $\text{Al}_9\text{Mn}_3\text{Si}$  are shown in figure 10. A pseudogap in the {Al + Si} DOS is clearly seen. This large pseudogap is mainly characteristic of a  $p$  band at this energy, but the pseudogap in the total DOS is narrower. In Ref. [38], we have shown that the pseudogap in  $sp$  DOS is due to the scattering of  $sp$  states by the Mn sub-lattice (called Mn(1) sub-lattice) via a strong  $sp$ - $d$  hybridization. To analyze

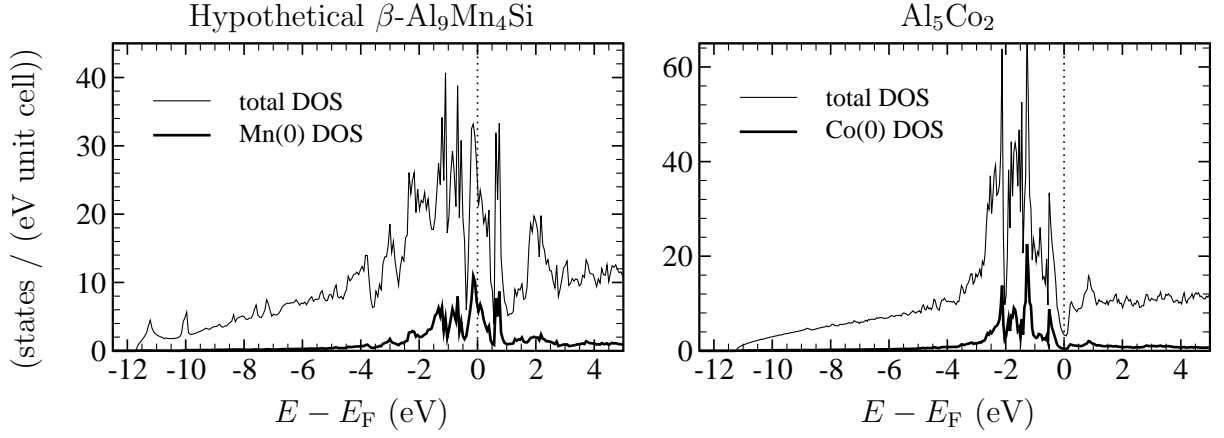


Figure 11: LMTO DOSs of the almost isomorphous hypothetical  $\beta$ - $\text{Al}_9\text{Mn}_3\text{Si}$ , and actual  $\text{Al}_5\text{Co}_2$ . (see text)

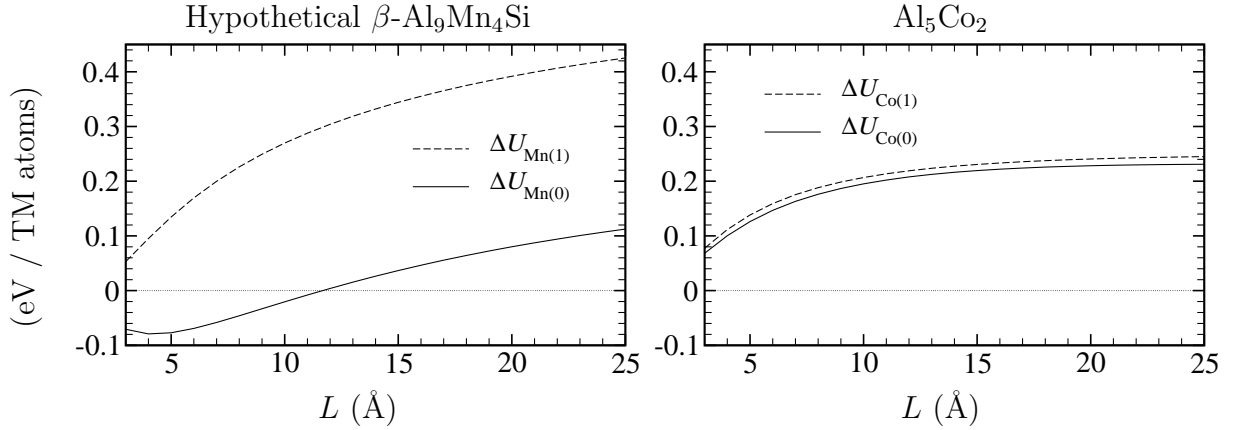


Figure 12: Variation of the structural energy  $\Delta U$  due to the effective TM–TM interaction in the almost isomorphous hypothetical  $\beta$ - $\text{Al}_9\text{Mn}_3\text{Si}$ , and actual  $\text{Al}_5\text{Co}_2$ . (see text) [38]

the origin of the vacancy in  $\beta$  phases, we have performed calculation including a new Mn atom, called Mn(0), on site (2d) in  $\beta$ - $\text{Al}_9\text{Mn}_3\text{Si}$  structure. Atomic positions and lattice parameters are those of  $\beta$ - $\text{Al}_9\text{Mn}_3\text{Si}$ . This hypothetical phase is named  $\beta$ - $\text{Al}_9\text{Mn}_4\text{Si}$ . The absence of pseudogap in the total DOS (figure 11) shows a the great effect on Mn(0) which is very different from the one of Mn(1). Indeed Mn(1) (on site (6h)) creates the pseudogap in  $\beta$ - $\text{Al}_9\text{Mn}_3\text{Si}$  DOS, whereas Mn(0) destroys it in hypothetical  $\beta$ - $\text{Al}_9\text{Mn}_4\text{Si}$  total DOS. Thus Mn(0) on site (2d) “fills up” the pseudogap via the  $sp$ - $d$  hybridization; whereas Mn(1) on site (6h) enhances the pseudogap. A similar result is obtained for hypothetical  $\varphi$ - $\text{Al}_{10}\text{Mn}_4$ , by putting Mn(0) in place of the vacancy in  $\varphi$ - $\text{Al}_{10}\text{Mn}_3$  phases. This illustrates clearly the non-trivial effect of the Mn positions on the electronic structure of  $spd$  Hume-Rothery alloys.

On the other hand, Co(0) on site (2d) increases the pseudogap (figure 11) in  $\text{Al}_5\text{Co}_2$ .



Table 3: Inter-atomic distances around the site (2d) in  $\beta$ -Al<sub>9</sub>Mn<sub>3</sub>Si,  $\varphi$ -Al<sub>10</sub>Mn<sub>3</sub> and Al<sub>5</sub>Co<sub>2</sub>. TM(1) is either Mn(1) or Co(1).  $X$  corresponds to the vacancy Va in  $\beta$ ,  $\varphi$  phases, and to Co(0) in Al<sub>5</sub>Co<sub>2</sub>.

Neighbors	Distances (Å)		
	$\beta$ Al <sub>9</sub> Mn <sub>3</sub> Si	$\varphi$ Al <sub>10</sub> Mn <sub>3</sub>	Al <sub>5</sub> Co <sub>2</sub>
3 Al	2.72	2.77	2.61
6 Al	2.23	2.29	2.35
6 TM(1)*	3.81	3.82	3.86

\* Atom in (2d) and TM(1) are not first-neighbor.

## 5.2 Medium-range Mn–Mn interaction can induce vacancies in the atomic structure

To understand the origin of the vacancy (Va) in  $\beta$  and  $\varphi$  structure, it is not enough to analyze the local environment (first neighbor environment). Indeed, the local environment around vacancy (table 3), is very similar [38] to that of Co(O) in Al<sub>5</sub>Co<sub>2</sub> and that of Mn(0) in hexagonal  $\mu$ -Al<sub>4.12</sub>Mn [36] and  $\lambda$ -Al<sub>4</sub>Mn [37]. Therefore we have considered the medium-range TM–TM interactions.

For phases containing several TM Wyckoff sites, the effective TM–TM interaction allows to compare the relative stability of TM atoms on different Wyckoff sites. Considering the hypothetical  $\beta$ -Al<sub>9</sub>Mn<sub>4</sub>Si phase (see previous paragraph), the variation,  $\Delta U_{\text{Mn}}$ , of  $U$  is determined when one Mn atom (Mn<sub>*i*</sub>) is removed from the structure and is put as an impurity in an Al matrix:

$$\Delta U_{\text{Mn}_i} = - \sum_{k (k \neq i)} \Phi_{\text{Mn-Mn}}(r_{ik}) e^{-\frac{r_{ik}}{L}}. \quad (14)$$

$\Phi_{\text{Mn-Mn}}$  is the effective TM–TM interaction (figure 8);  $r_{ik}$ , the Mn<sub>*i*</sub>–Mn<sub>*k*</sub> distance; and  $L$ , the mean-free path due to static disorder or/and phonons. Mn atoms on the same Wyckoff sites have the same  $\Delta U_{\text{Mn}}$  value, Mn atoms on different Wyckoff sites have different  $\Delta U_{\text{Mn}}$  values that can be compared. The most stable Mn Wyckoff sites correspond to the highest  $\Delta U_{\text{Mn}(k)}$  values. As previously, the energy is calculated from equation (14) without the first-neighbor Mn–Mn contributions in order to analyze effects at medium-range order.

For hypothetical  $\beta$ -Al<sub>9</sub>Mn<sub>4</sub>Si (where Mn(0) replaces the vacancy), one finds:  $\Delta U'_{\text{Mn}(1)} > \Delta U'_{\text{Mn}(0)}$  (figure 12). Mn(0) in (2d) is therefore less stable than Mn(1) in (6h) in the hypothetical  $\beta$ -Al<sub>9</sub>Mn<sub>4</sub>Si, in agreement with the fact that (2d) site is empty (vacancy) in  $\beta$ -Al<sub>9</sub>Mn<sub>3</sub>Si phase. A similar result was obtained for the hypothetical  $\varphi$ -Al<sub>10</sub>Mn<sub>4</sub>.

Al<sub>5</sub>Co<sub>2</sub> phase is almost isomorphic of  $\beta$  and  $\varphi$  phases, but there is a Co site (Co(0)) corresponding to the vacancy of  $\beta$  and  $\varphi$ .  $\Delta U_{\text{Co}(0)}$ , calculated with the effective Co–Co interaction, is almost equal to  $\Delta U_{\text{Co}(1)}$  (figure 12), thus Co(0) in (2d) is as stable as Co(1) in (6h). This justifies why no vacancy exists in Al<sub>5</sub>Co<sub>2</sub>.

The difference between  $\varphi$ ,  $\beta$  phases, and Al<sub>5</sub>Co<sub>2</sub> phase, is understood by considering the TM–TM effective interaction  $\Phi_{\text{TM-TM}}$  (figure 8). In  $\varphi$ ,  $\beta$  phases, the environment of Va contains two Mn atoms at the distance 3.8 Å (table 3). Similarly, in Al<sub>5</sub>Co<sub>2</sub> the environment of Co(0) contains two Co at the distance 3.8 Å.  $\Phi_{\text{Mn-Mn}}(3.8 \text{ Å}) > 0$ , then 3.8 Å corresponds to an unfavorable Mn–Mn distance; whereas  $\Phi_{\text{Co-Co}}(3.86 \text{ Å}) < 0$ , then 3.86 Å corresponds to a favorable Co–Co distance.

Finally, we have compared [38] the case of  $\beta$ ,  $\varphi$  phases with the hexagonal  $\mu$ -Al<sub>4.12</sub>Mn [36] and  $\lambda$ -Al<sub>4</sub>Mn [37] that contain an atomic site with a very similar environment to that of Va in  $\beta$ ,  $\varphi$ . From X-ray data, this site is occupied by a Mn (Mn(0)) in  $\mu$ ,  $\lambda$ . That difference with  $\beta$   $\varphi$  cannot be explained in term of local environment whereas the medium-range Mn–Mn interaction explains it [38]. Indeed, in  $\mu$ ,  $\lambda$  there is no Mn(0)–Mn distance equal to 3.8 Å, but the first Mn(0)–Mn distance is 4.8 Å which corresponds to a favorable Mn–Mn spacing (figure 8).

## 6 Magnetism of Al(Si)–Mn phases

### 6.1 Introduction and ab initio studies of magnetism

The Mn impurity in Al host is close to a magnetic / non-magnetic transition. But the situation in Al–Mn alloys is rather different as most of Mn atoms are non-magnetic. Indeed, it is found experimentally that in simple crystals Mn is non-magnetic, and in complex phases and approximants only a small proportion of Mn is magnetic (F. Hippert, V. Simonet et al. [39, 40, 41, 42, 43], C. Berger and J.J. Préjean et al. [44, 45])

The LMTO calculations confirm that Al<sub>12</sub>Mn,  $\alpha$ -Al<sub>6</sub>Mn,  $\varphi$ -Al<sub>10</sub>Mn<sub>3</sub>,  $\beta$ -Al<sub>9</sub>Mn<sub>3</sub>Si,  $\alpha$ -Al–Mn–Si, Al<sub>11</sub>Mn<sub>4</sub>, Al<sub>13</sub>Mn<sub>4</sub> (Al<sub>13</sub>Fe<sub>4</sub> structure) are non-magnetic. The fact that Mn atoms are not close to a magnetic / non-magnetic transition is shown by the effect of the dilatation (figure 13). For instance in the case of Al<sub>6</sub>Mn an isotropic dilation of lattice parameters of  $\sim 8\%$  is necessary to reach the magnetic transition, whereas an Mn in substitution in the Al matrix (Al f.c.c.) is on the magnetic / non-magnetic transition.

In the magnetic complex Al–Mn–(Pd)–(Si) phases, LMTO calculations show that some Mn are non-magnetic and other Mn are magnetic (Al–Mn approximants [46], Al–Pd–Mn approximants [47], 1/1-Al<sub>65.9</sub>Pd<sub>12.2</sub>Mn<sub>14.6</sub>Si<sub>7.3</sub> [39],  $\mu$ -Al<sub>4.12</sub>Mn [16]). These calculations suggest also that the magnetic Mn atoms are located on Mn sites less stable than the Mn sites occupied by non-magnetic Mn.

Up to now, most of the theoretical studies have focused on the role of the local environment of the Mn atoms to explain the occurrence of localized magnetic moment like in the case of Mn impurity in the Al matrix (see Refs. in [48]). In particular, clusters calculations have shown that the local symmetry and the first-neighbor distance can have a strong influence. Vacancies, Mn pairs or Mn triplets or Mn quadriplets are also often invoked to explain magnetic moments [39, 42, 43]. However, in crystals and quasicrystals, most of Mn atoms are non-magnetic in spite of various environments including pairs, triplets and quadriplets. It is therefore expected that local environment properties are not enough to understand the existence of localized magnetic moment in Al–Mn compounds [48].

Theoretical works have focused on the occurrence of local moments in a series of Al–Mn alloys [49, 46]. The authors conclude that the crystal  $\alpha$ -Al<sub>6</sub>Mn is non-magnetic because of a pseudogap in the local density of states (DOS) at the Fermi energy which is of a Hume–Rothery type. Because of the chemical disorder, a solid solution at the same concentration (on an Al f.c.c. lattice without relaxation) presents a very different electronic DOS, without a pseudogap at the Fermi energy [46]. In this solution the Mn atoms are magnetic. In the Hume–Rothery mechanism, the pseudogap contributes to the stabilization of crystals, thus magnetic state of Mn atoms is related to the stabilization mechanism.

An illustration of the effect of a strong effective Mn–Mn interaction on magnetism has been given by an LMTO calculation on  $\beta$ -Al<sub>9</sub>Mn<sub>3</sub>Si and  $\varphi$ -Al<sub>10</sub>Mn<sub>3</sub> [48]. The hexagonal

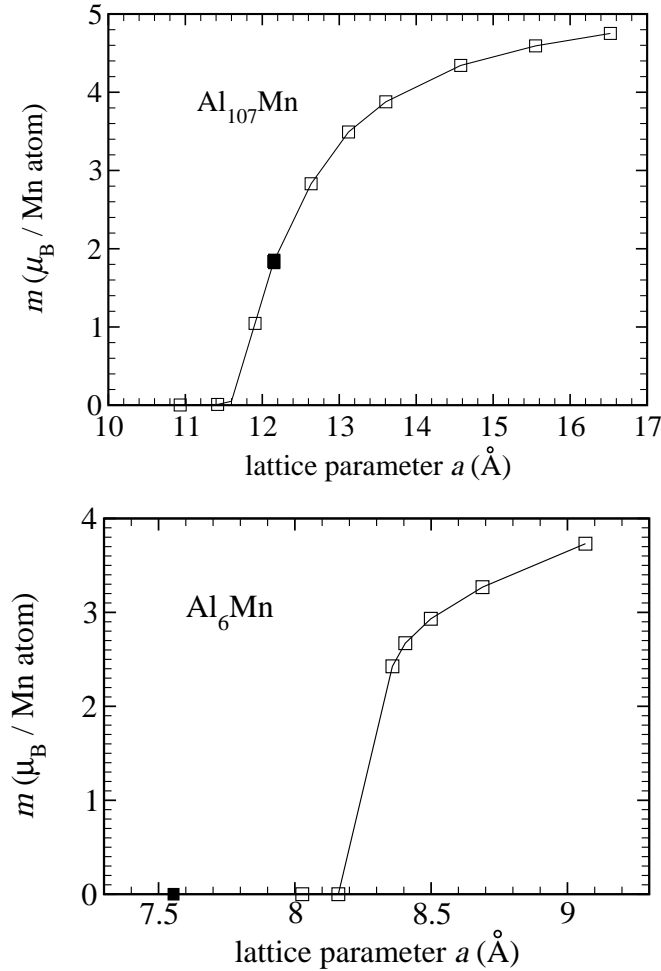


Figure 13: Local moment on Mn atoms in a cubic  $\text{Al}_{107}\text{Mn}$  model (impurity model) and  $\text{o-Al}_6\text{Mn}$ , versus the lattice parameter of the cubic lattice (isotropic dilatation). The black square corresponds to the experimental lattice parameter of f.c.c. Al and  $\text{o-Al}_6\text{Mn}$ , respectively. Lines are guides for the eyes.

unit cell of these phases, contains two isolated Mn-triplets. The Mn atoms belonging to the same triplet are first-neighbors, but each Mn-triplet is surrounded by Al(Si) atoms only. LMTO calculations show that the Mn-triplets are non-magnetic. In order to determine the role of the effective Mn–Mn interaction on this result, we performed a calculation for an hypothetical  $\beta\text{-Al}_9\text{Mn}_{1.5}\text{Cu}_{1.5}\text{Si}$  phase, constructed from  $\beta\text{-Al}_9\text{Mn}_3\text{Si}$  by replacing one Mn-triplet by a Cu-triplet in each cell. The Cu has no medium-range interaction as its  $d$  orbitals are full and it has almost the same number of valence ( $sp$ ) electrons as Mn. Thus the Fermi energy is essentially unchanged as well as the local environment of the Mn-triplet. Yet the LMTO results show a magnetic moment equal to  $\sim 1 \mu_{\text{B}}$  on each Mn in  $\beta\text{-Al}_9\text{Mn}_{1.5}\text{Cu}_{1.5}\text{Si}$  (the 3 Mn atoms in a triplet are almost equivalent with a ferromagnetic spin orientation). This is a proof that the magnetic state of an Mn atom is sensitive to Mn atoms at a distance of  $\sim 5 \text{ \AA}$  (distance between two Mn-triplet in  $\beta$ -phase). The energy of formation of magnetic moments in  $\beta\text{-Al}_9\text{Mn}_{1.5}\text{Cu}_{1.5}\text{Si}$  is  $-0.046 \text{ eV}$  per triplet. Similar results are obtained for  $\varphi\text{-Al}_{10}\text{Mn}_3$ . These results confirm that an magnetic state is expected for an isolated Mn-triplet in Al matrix, but in  $\beta$  and  $\varphi$ , a strong inter-triplets

Mn–Mn interaction maintains a non-magnetic state.

## 6.2 The magnetic Mn–Mn effective interaction

The magnetic effective Mn–Mn interaction in Al(rich) alloys is calculated as follows [48]. The  $d$  orbitals of Mn atoms are coupled to free states (Al states mainly) but we neglect the direct  $d$ – $d$  coupling. The local magnetic moment is treated in a mean-field type approach as in band-structure calculations. That is one neglects spin fluctuations effect. We now consider the energy  $E$  of 2 Mn atoms (Mn<sub>1</sub> and Mn<sub>2</sub>) in an Al matrix which is simulated by the jellium (free electron).  $E$  is a function of the Mn<sub>1</sub>–Mn<sub>2</sub> distance,  $r_{12}$ , and of the moments  $m_1$  and  $m_2$  carried by the 2 Mn, respectively. By convention we choose  $E(r_{12} = \infty, m_1 = m_2 = 0) = 0$ . Then one may write [48]:

$$E(r_{12}, \vec{m}_1, \vec{m}_2) = E_1(m_1) + E_1(m_2) + \Phi_{\text{Mn–Mn}}(r_{12}, \vec{m}_1, \vec{m}_2) \quad (15)$$

$E_1(m_i)$  is the energy of one Mn<sub>i</sub> impurity in an Al matrix (Virtual Bound State), it does not depend on the position of Mn<sub>i</sub>.  $\Phi_{\text{Mn–Mn}}$  is an effective Mn–Mn interaction which is mediated by the  $sp$  states, and it depends on Mn–Mn distance and the moments carried by the Mn atoms.

As Mn impurity is close to the magnetic transition,  $E_1(m)$  is small ( $|E_1(m)| \lesssim 0.05$  eV). The value of  $E_1(m)$ , has been estimated from LMTO calculation for the concentration Al<sub>107</sub>Mn (Mn atoms substituting Al atoms in a Al f.c.c. lattice, without inter-atomic distance relaxation): Mn is found magnetic with a  $1.8 \mu_B$  moment and the gain in energy for one Mn atom to become magnetic is  $E_1(m = 1.8 \mu_B) \simeq -0.05$  eV.

We have calculated  $\Phi$  for two magnetic Mn atoms (2  $d$  orbitals) in free electron matrix (figure 14) [48]. A remarkable feature is that most pronounced minima in the Mn pair interaction correspond to non-magnetic Mn pairs for specific Mn–Mn spacings. Therefore the most stable Mn sites should be occupied by non-magnetic Mn. When Mn are in a less stable position, it could be magnetic. This conclusion is consistent with experimental results from which most of the Mn atoms are non-magnetic, whereas only particular sites (or defect) could lead to magnetic Mn.

For small moments, the Mn pair interaction energy can be developed as:

$$\Phi_{\text{Mn–Mn}}(r_{12}, m_1, m_2) = a(r_{12}) + \frac{1}{2} b(r_{12}) (m_1^2 + m_2^2) + c(r_{12}) \vec{m}_1 \cdot \vec{m}_2 + \dots \quad (16)$$

The  $a(r)$  terms is the Mn–Mn interaction for non-magnetic Mn atoms ( $m_1 = m_2 = 0$ ) (figure 8). The  $c(r)$  term is the RKKY exchange interaction between the two spins. The  $b(r)$  term plays a central role in our study of the existence of local magnetic moments in a non-magnetic environment. As an example, let us consider the magnetic moment  $m_1$  of an atom Mn<sub>1</sub> interacting with a non magnetic Mn<sub>2</sub> ( $m_2 = 0$ ), in the Al matrix. We neglect  $E_1(m_1)$  which is small. The interaction between Mn<sub>1</sub> and Mn<sub>2</sub> depends on the magnetic moment  $m_1$  carried by Mn<sub>1</sub> via the term  $b(r_{12})$ :  $\Phi_{\text{Mn–Mn}}(r_{12}, m_1 = 0, m_2) = a(r_{12}) + \frac{1}{2} b(r_{12}) m_1^2$ . The minimum of  $\Phi_{\text{Mn–Mn}}$  (stable) is reached for a  $m_1$  value that depends on the sign of  $b(r_{ij})$ : For  $b(r_{ij}) < 0$ , stable Mn<sub>1</sub> is magnetic, whereas for  $b(r_{ij}) > 0$  stable Mn<sub>1</sub> is non-magnetic. Therefore, the term  $b(r)$  implies that the formation of a magnetic moment is sensitive to the presence of other non-magnetic Mn.

We now consider the general case of more than 2 Mn atoms in Al matrix. Starting from non-magnetic case, we calculate the formation energy,  $\Delta\mathcal{E}_i$ , for the moment,  $m_i$ , on

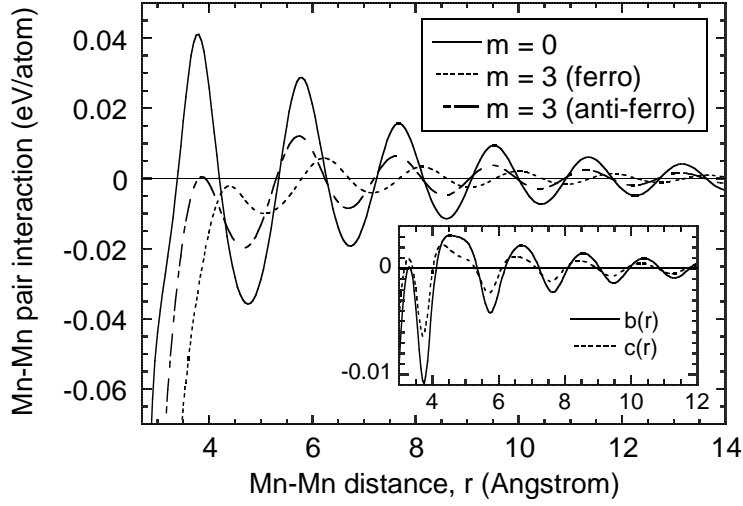


Figure 14: Effective Mn–Mn interaction  $\Phi_{\text{Mn-Mn}}$  in Al host (free electrons). Non-magnetic case ( $m_1 = m_2 = 0$ ); magnetic case: the two moments ( $m_1 = m_2 = 3 \mu_B$ ) alignment is anti-ferromagnetic or ferromagnetic. [Inset: Coefficients  $b(r)$  and  $c(r)$  (equation(16)),  $a(r) = \Phi(m_1 = m_2 = 0)$ .]

the atom  $\text{Mn}_i$ :

$$\Delta \mathcal{E}_i = E_1(m_i) + \mathcal{B}_i m_i^2 \quad \text{with} \quad \mathcal{B}_i = \sum_j \frac{b(r_{ij})}{2} e^{-\frac{r_{ij}}{L_0}}. \quad (17)$$

$r_{ij}$  is the  $\text{Mn}_i$ – $\text{Mn}_j$  distances.  $E_1$  include all first neighbors effects. The sum  $\mathcal{B}_i$  takes into account the medium-range effects of the Mn–Mn interaction. When  $|\mathcal{B}_i m_i^2| > |E_1(m_i)|$ , the sign of  $\mathcal{B}_i$  determines the magnetic states of  $\text{Mn}_i$ :

$$\mathcal{B}_i > 0 \implies \text{Mn}_i \text{ is non-magnetic } (m_i = 0) \quad (18)$$

$$\mathcal{B}_i < 0 \implies \text{Mn}_i \text{ is magnetic } (m_i \neq 0) \quad (19)$$

For all Mn atoms in  $\alpha$ - $\text{Al}_6\text{Mn}$ ,  $\alpha$ - $\text{Al}_{73}\text{Mn}_{17}\text{Si}_{10}$ ,  $\beta$ - $\text{Al}_9\text{Mn}_3\text{Si}$ ,  $\text{Al}_3\text{Mn}$  phases, we found  $\mathcal{B}_i > 0.015\text{eV}$  when  $L_0 > 20 \text{ \AA}$  (figure 15). Assuming  $|E_1| \leq 0.05 \text{ eV}$  for  $m \simeq 2 \mu_B$ ,  $\Delta \mathcal{E}$  is minimized when Mn are non-magnetic, as found experimentally.

In liquid phases the situation is completely different. Because of the loss of the medium range order,  $\mathcal{B}_i \simeq 0$ . Then thermal expansion, displacements of the atoms and spin fluctuations, should favor a non zero average moment as found experimentally [41] and by numerical simulations [49, 46].

We have also shown that  $\mathcal{B}$  interaction between atoms of different Mn triplets plays a central role in  $\beta$ - $\text{Al}_9\text{Mn}_3\text{Si}$  [48, 13]. This interaction forbids the occurrence of Mn moments in triplets, whereas a single Mn triplet in an Al matrix should be magnetic.

## 7 Electronic localization

### 7.1 Electronic transport

T. Fujiwara *et al.* have first shown that the electronic structure of Al–TM approximants and related phases is characterized by two energy scales [8, 9, 50, 51, 52]. The largest,

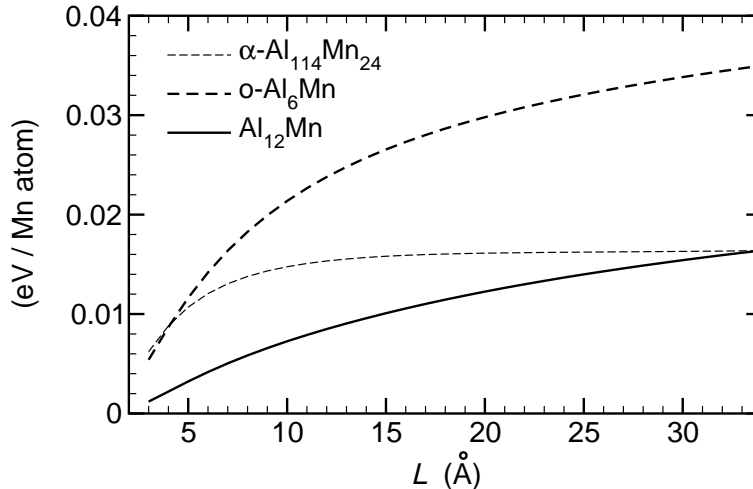


Figure 15:  $\mathcal{B}_{\text{Mn}}(L)$  for  $\alpha\text{-Al}_{110}\text{Mn}_{24}$ ,  $o\text{-Al}_6\text{Mn}$ , and  $\text{Al}_{12}\text{Mn}$  [13]. In these crystals, Mn atoms are not first-neighbor.

about  $0.5 - 1$  eV, is the width of the pseudogap near the Fermi energy  $E_{\text{F}}$ . It is related to the Hume–Rothery stabilization via the scattering of electrons by the TM sub-lattice because of a strong  $sp$ – $d$  hybridization. The smallest, less than 0.1 eV, is characteristic of the small dispersion of the band energy  $E(\mathbf{k})$  [50]. This energy scale seems more specific to phases related to the quasiperiodicity. The first consequence as far as the transport is concerned is a small velocity at Fermi energy

$$v(E_{\text{F}}) = \left( \frac{\partial E}{\partial k} \right)_{E=E_{\text{F}}} . \quad (20)$$

From LMTO calculations the Bloch–Boltzmann conductivity  $\sigma_{DC}$  (intra-band conductivity) is evaluated in the relaxation time approximation. With a realistic value of scattering time,  $\tau \sim 10^{-14}$  s [54], one obtain  $\sigma_{DC} \sim 300 - 1000 (\Omega\text{cm})^{-1}$  for a  $\alpha\text{-Al-Mn}$  model [50] and  $1/1\text{-Al-Fe-Cu}$  model [51]. These value correspond to the measured values [44] which are anomalously low for metallic alloys. For decagonal approximant the anisotropy found experimentally in the conductivity is also reproduced correctly [52].

The semi-classical Bloch–Boltzmann description of transport gives interesting results for the intra-band conductivity in crystalline approximants, but it is insufficient to take into account most of the aspect due to the special localization of electrons due to the quasiperiodicity [53]. Some specific transport properties like the temperature dependence of the conductivity (inverse Mathiessen rule, the defects influence, the proximity of with a metal / insulator transition) requires to go beyond a Bloch–Boltzmann analysis. In fact, two different unconventional transport mechanisms specific of these materials have been proposed [54, 50, 53, 55]. Transport could be dominated, for short relaxation time  $\tau$  by hopping between “critical localized states”, whereas for long time  $\tau$  the regime could be dominated by non-ballistic propagation of wave packets between two scattering events.

The experimental optical conductivity of quasicrystals and approximants is also unusual. The real part of the conductivity increases linearly with the energy at low energies (below 1 eV), and there is no Drude peak. The absence of a Drude peak in approximants should be due to the small DOS and the very low intra-band conductivity. T. Fujiwara et al. [50] calculated the optical conductivity due to the inter-band transition from the LMTO

band dispersion of  $\alpha$ -Al–Mn. It reproduces the linearity and the peak position observed. More recently, D. Mayou [56] derived a generalized Drude formula for the optical conductivity of quasicrystals. It shows how a non-ballistic propagation due to the quasiperiodicity can affect the optical properties and explains the absence of a Drude peak, the increase of conductivity with disorder, and the inverse Mathiessen rule.

To conclude, it appears that the degradation of the metallic character can be obtained either by a localization of states or by a decrease of the DOS (semi-conducting state). It seems that quasicrystals and approximants with large unit cell combine both effects and this explains their unusual transport properties.

## 7.2 Cluster virtual bound states

The very low conductivity of quasicrystals and approximants in spite of the non zero density of states at the Fermi level, shows that electrons tend to be localized in a particular way.

The electronic structure of quasiperiodic lattices has been studied theoretically within two different approaches. The first consist in the analysis of the spectral properties of quasiperiodic model Hamiltonian. This approach shows the existence of a new kind of states called critical states. Those states, which are neither localized (like in doped-semiconductors) nor extended (like in crystals), are characterized by the particular localization due the long range quasiperiodic order.

The second approach to study the electronic properties of quasicrystals consist in the study of realistic approximants of quasicrystals. By this way, we analyze the effect of the local atomic order (chemical and topological local order) on the quasicrystal properties. Band structure calculations for approximants reveal that dispersion relations are flat, corresponding to small velocities. Fine peaks in the density of states (DOS) are associated with the flat bands. Experimental results on transport properties show that quasicrystals Al–Pd–Mn and Al–Cu–Fe and their periodic approximants present very similar properties. This suggests that the electronic transport in these alloys is essentially determined by the local atomic order on the length scale of the lattice parameter of the approximants, i.e.  $10 - 30 \text{ \AA}$ .

As for the local atomic order, one of the characteristics of the quasicrystals and approximants, is the occurrence of atomic clusters [58]. Nevertheless the clusters are not well defined because some of them overlap each other, and they are a lot of glue atoms. These remarks lead us to consider that clusters are not isolated but they are embedded in metallic medium. Our aim was to check whether the scattering of electrons by cluster, on a scale of  $10-30 \text{ \AA}$ , can localize electrons.

Our model [22, 23] is based on a standard description of inter-metallic alloys. The central quantity is the transfer matrix ( $\mathbf{T}$  matrix) of one cluster. Considering the cluster embedded in a metallic medium, we calculated the variation  $\Delta n(E)$  of the DOS due to the cluster (Lloyd formula). For electrons, which have energy in the vicinity of  $E_F$ , transition atoms (such as Mn and Fe) are strong scatterer whereas Al atoms are weak scatterer. Then, following a classical approximation, we neglected the potential of Al atoms.

In the figure 16, the variation  $\Delta n(E)$  of the DOS due to different clusters are shown. The Mn icosahedron is the actual Mn icosahedron of the  $\alpha$ -Al–Mn–Si approximant. As an example of a larger cluster, we consider one icosahedron of Mn icosahedra, which might appeared in the structural model for quasicrystals.

$\Delta n(E)$  of clusters exhibits strong deviations from the Virtual Bound State corresponding to one Mn atom. Indeed several peaks and shoulders appear. The width of the most

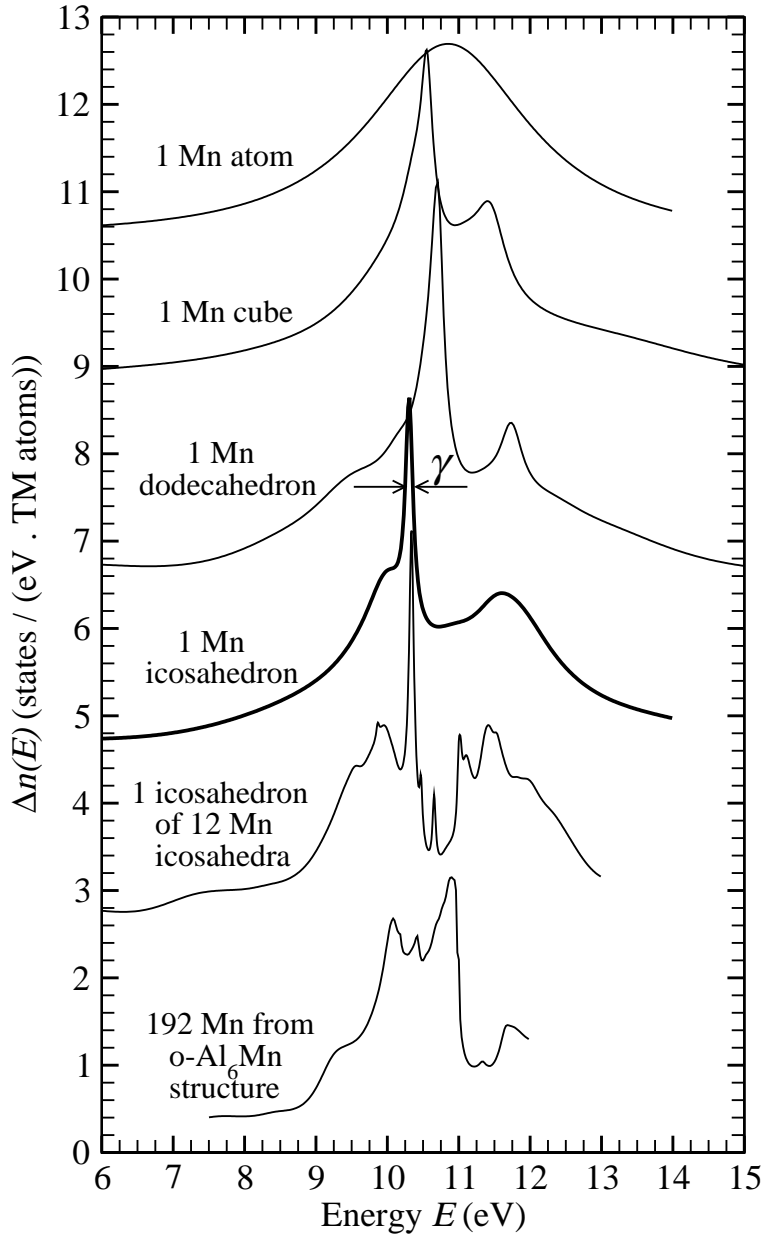


Figure 16: Variation  $\Delta n(E)$  of the DOS due to Mn clusters in the Al matrix. In these clusters the first-neighbors Mn–Mn distances are larger than  $4.50 \text{ \AA}$ . Diameters  $D$  of small clusters:  $D(\text{cube}) = 3.90 \text{ \AA}$ ,  $D(\text{icosahedron}) = 9.21 \text{ \AA}$  (actual value in  $\alpha\text{-Al-Mn-Si}$ ,  $D(\text{dodecahedron}) = 12.33 \text{ \AA}$ . The icosahedron of 12 Mn icosahedra is obtained after an inflation by a factor  $\tau^2$  of an initial Mn icosahedron, so the diameter of the icosahedron of Mn icosahedra is  $\sim 33 \text{ \AA}$  and it contains 144 Mn atoms.

narrow peaks ( $50 - 100 \text{ meV}$ ) are comparable to the fine peaks of the calculated DOS in the approximants. Each peak corresponds to a resonance due to the scattering by the cluster. This is associated to states “localized” by the cluster. They are not eigenstate, they have finite lifetime of the order of  $\hbar/\gamma$ , where  $\gamma$  is the width of the peak. Therefore, the stronger the effect of the localization by cluster is, the narrower is the peak. The large lifetime is the proof of a localization, but in the real space these states have an extension on length scale of the cluster, typically  $\sim 9.21 \text{ \AA}$  for Mn icosahedron that exist in the actual  $\alpha\text{-Al-Mn-Si}$



approximants. As an example we have considered also an icosahedron of 12 Mn icosahedra. The diameter of each Mn icosahedron is 9.21 Å too, and the diameter of the icosahedron of Mn icosahedra is  $\sim 33$  Å. The DOS of the large cluster contains new peaks with respect to the simple Mn icosahedron (figure 16). These are states localized on the length scale of about 33 Å. Therefore, in this large cluster, some states are localized on the length scale of the Mn icosahedron and other states are localized on the length scale of the icosahedron of Mn icosahedra.

We named this new kind of electronic states the “*cluster virtual bound states*”, by analogy with the Virtual Bound States of Friedel [5]-Anderson [6] for a TM impurity. Indeed, the physical origin of these states can be understood as follows. Consider incident electrons, with energy  $E$  close to  $E_F$ , scattered by the cluster. In Al–Mn alloys  $E_F \simeq E_d$ , where  $E_d$  is the energy of the  $d$  orbital. In this energy range, the potential of the Mn atom is strong and the Mn atoms can roughly be consider as hard spheres with radius of the order of the  $d$  orbital size ( $\sim 0.5$  Å). An effect similar to that of the “Faraday cage” can confine electrons in the cluster provided that their wavelength  $\lambda$  satisfies  $\lambda \gtrsim l$ , where  $l$  is the distance between two hard spheres (TM–TM distances). In the case of  $\alpha$ -Al–Mn–Si,  $l \simeq 3.6$  Å (if we assume a free electron band and  $E_F = 10.33$  eV) and the distance  $l$  is about 3.8 Å. Consequently, we expected to observe such a confinement. This effect is a multiple scattering effect, and it is not due to an overlap between  $d$  orbitals because Mn atoms are not first-neighbor.

We have also shown that these resonances are very sensitive to the geometry of the cluster. For instance, they disappear quickly when the radius of the Mn icosahedron increases, or when the Mn icosahedron is truncated [23].

### 7.3 Band-gap in some Al–TM alloys

While alloys composed of metallic constituents are expected to be metallic, several Al–TM phases are semi-conducting phases with a band-gap smaller than traditional semiconductors (less than 1 eV). Experimental measurements of transport properties and optical properties indicate the presence of a small gap in the DOS of the orthorhombic Al<sub>2</sub>Ru (C54 structure) [57]. Its width is expected to be  $\sim 0.17$  eV. This band-gap (or a very deep pseudogap) has been confirmed theoretically from our first-principles calculations [19] and then other groups (see Refs. in [13]). All these works conclude that the band-gap is due the  $sp$ - $d$  hybridization, but not to charge transfers which are small [19]. The DOS of Al<sub>2</sub>Ru is shown on figure 17. A strong  $p(\text{Al})$ - $d(\text{Ru})$  hybridization for electrons near  $E_F$  has also been confirmed by photo-emission spectroscopy [59].

As shown recently by M. Krajeć and J. Hafner [60] from first-principles, the semi-conducting gap in Al<sub>2</sub>TM DOS does not disappear if TM sites are occupied by two different TM elements (TM<sub>1</sub> and TM<sub>2</sub>), provided that the electron per atom ratio is conserved. These phases have hypothetical structures and thus this does not prove that actual phases with the same composition are semi-conducting phases. From a detailed analysis of the ab initio calculations, the authors have shown an enhanced charge density halfway between certain first-neighbor pairs of atoms, and a bonding / anti-bonding splitting of the electronic states. This suggests a dominantly covalent character of the bond between atoms due to  $sp$ - $d$  hybridized orbitals.

A narrow gap may also be found in some hypothetical Al(Si)–Mn phases. Indeed, for particular positions of the Si atoms in the  $\alpha$ -Al–Mn–Si phase, a very narrow gap at  $E_F$  has been predicted very recently by E.S. Zijlstra and S.K. Bose [61]. We calculated [13]

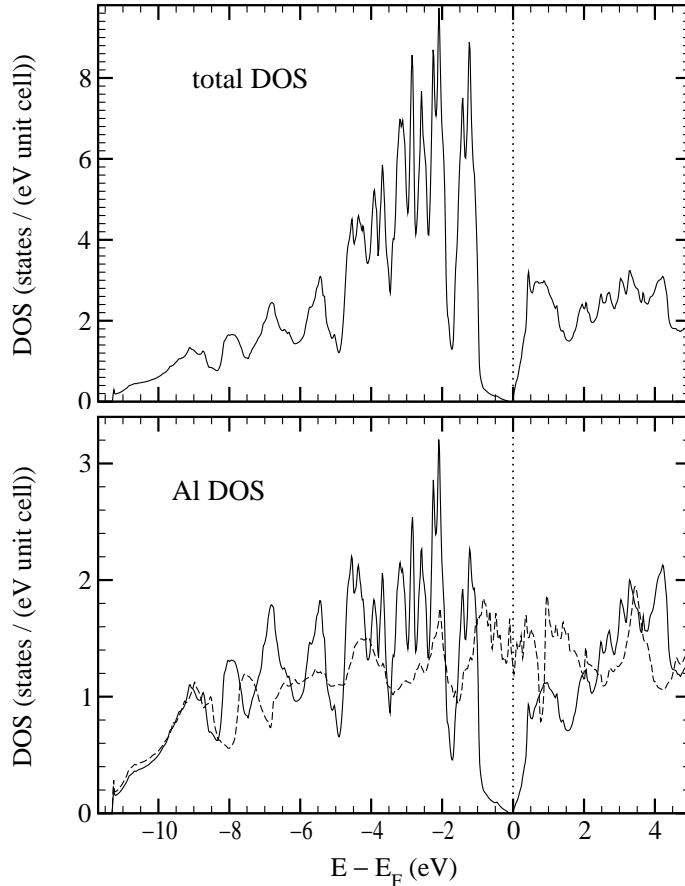


Figure 17: LMTO total DOS and Al local DOS of the orthorhombic  $\text{Al}_2\text{Ru}$ . Dashed line: calculation without  $sp$ - $d$  hybridization. [19]

DOS of  $\delta\text{-Al}_{11}\text{Mn}_4$  with the atomic structure proposed by Kontio *et al.* (triclinic,  $P\bar{1}$ ). It exhibits a gap at energy close to  $E_F$ . According to recent structure refinement this triclinic structure proposed is not a good refinement of the crystallographic data. But, it gives an interesting example for a possible band-gap in Al(rich)–Mn materials.

## 8 Conclusion

Our theoretical studies on Al(rich)–transition-metal (TM) alloys lead to consider these aluminides as  $spd$  electron phases, where a specific electronic structure governs the stability, the electronic properties and the magnetism. Schematically, the conduction states of these compounds could be seen like  $sp$  free states (mainly Al states) scattered by the strong potential of the TM atoms ( $d$  orbitals). The large value of the electronic density of the conduction electrons ( $\sim 3$  conduction electrons per Al atoms) creates strong Friedel oscillations of the charge density around each TM atoms. Consequently, effective TM–TM interactions mediated by the  $sp$  states are essential over medium-range distances (typically 10–20 Å). In agreement with a Hume-Rothery minimization of the band energy, these oscillating interactions leads to “frustration” mechanism which favors complex atomic structures (including quasicrystals and approximants phases). Indeed, a specificity of these compounds is that the stability (or not) of a TM atom on a given atomic site does not

depend only on the local environment, but it depends also on TM–TM interactions over distances larger than the first-neighbor distances. This can explain preferred TM–TM spacings in Al(rich)–TM alloys and the occurrence of atomic vacancies. The occurrence of localized magnetic moments carried by the TM atoms depends also on TM position via the TM–TM interactions. Our studies of the density of states gives also a simple explanation of the long standing problem of the negative valence of TM atoms in these materials. The strong scattering of the *sp* states by the TM atoms could also “localize” conduction states on atomic clusters with diameter of 10–30 Å and even more. In some cases the system might go to a semi-conducting regime with a gap in the density of states. This gap is also due to the scattering of *sp* states by *d* orbitals.

## 9 Acknowledgements

Our work owes much to the discussions with Prof. J. Friedel, Prof. T. Fujiwara, and Prof. D.G. Pettifor, and to their works in the field of the electronic structure of Hume–Rothery alloys. We are also grateful to many colleagues with whom we have collaborations: M. Audier, E. Belin–Ferré, C. Berger, R. Bellissent, A.M. Bratkovsky, F. Cyrot–Lackmann, F. Hippert, J.P. Julien, A. Pasturel, J.J. Préjean, L. Magaud, S. Roche and V. Simonet.

## References

- [1] G.V. Raynor, “Progress in the theory of alloys,” *Prog. Met. Phys.*, 1 (1949), 1.
- [2] W. Hume-Rothery, and G.V. Raynor, “The Structure of Metals and Alloys,” (London: Inst of Metals, 1954).
- [3] T.B Massalski, and U. Mizutani, “Electronic structure of Hume-Rothery phases,” *Prog. Mater. Sci.*, 22 (1978), 151-262.
- [4] A.T. Paxton, M. Methfessel, and D.G. Pettifor, “A bandstructure view of the Hume-Rothery electron phases,” *Proc. R. Soc. Lond. A*, 453 (1997), 1997, 1493-514.
- [5] J. Friedel, *Can. J. Phys.*, 34 (1956), 1190.
- [6] P.W. Anderson, “Localized Magnetic States in Metals,” *Phys. Rev.*, 124 (1961), 41-53.
- [7] J. Friedel, and F. Dénoyer, “Diffraction des rayons X par un mono-quasicristal Al–Li–Cu,” *C. R. Acad. Sci. Paris, Ser II*, 305 (1987), 171. J. Friedel, “Do metallic quasicrystals and associated Frank and Kasper phases follow the Hume Rothery rules?,” *Helv. Phys. Acta*, 61 (1988), 538.
- [8] T. Fujiwara, “Electronic structure in the Al–Mn alloy crystalline analog of quasicrystals,” *Phys. Rev. B*, 40 (1989), 942-6.
- [9] T. Fujiwara, and T. Yokokawa, “Universal pseudogap at Fermi energy in quasicrystals,” *Phys Rev Lett*, 66 (1991), 333.
- [10] A.P. Tsai, “Hume-Rothery rule for quasicrystalline compounds” in *The Science of Complex Alloy Phases*, Eds T.B. Massalski, E.A. Turchi (TMS publications, Warrendale, 2005) p. 201-214.

- [11] U. Mizutani, “Hume-Rothery rule in structurally complex alloy phases” in *The Science of Complex Alloy Phases*, Eds T.B. Massalski, E.A. Turchi (TMS publications, Warrendale, 2005) p. 1-42.
- [12] O.K. Andersen, “Linear methods in band theory,” *Phys. Rev. B*, 12 (1975), 3060-83.
- [13] G. Trambly de Laissardière, D. Nguyen Manh, and D. Mayou, “Electronic structure of complex Hume-Rothery phases and quasicrystals in transition-metal aluminides,” *Prog. Mater. Sci.*, 50 (2005) 679-788.
- [14] G. Trambly de Laissardière, D. Mayou, and D. Nguyen Manh, “Electronic Structure of Transition Atoms in Quasi-Crystals and Hume-Rothery Alloys,” *Europhys. Lett.* 21 (1993), 25-30.
- [15] G. Trambly de Laissardière et al., “Electronic structure and hybridization effects in Hume-Rothery alloys containing transition elements,” *Phys. Rev. B*, 52 (1995), 7920-7933.
- [16] D. Nguyen-Manh, and G. Trambly de Laissardière, “First-principles predictions of magnetic properties for a complex and strongly related to quasicrystalline phase:  $\mu$ -Al<sub>4</sub>Mn,” *J. Mag. Mag. Mater.*, 262 (2003), 496-501.
- [17] E. Belin-Ferré, and J.-M. Dubois, “Pseudo-gap and properties of Al-based complex and aperiodic compounds” in *The Science of Complex Alloy Phases*, Eds T.B. Massalski, E.A. Turchi (TMS publications, Warrendale, 2005) p. 281-324.
- [18] D. Nguyen-Manh et al., “On the phase stability of transition-metal trialuminide compounds,” *Intermetallic*, 3 (1995), 9-14.
- [19] D. Nguyen Manh et al., “Electronic Structure and Hybridization Effects in the Compounds Al<sub>2</sub>Ru and Ga<sub>2</sub>Ru,” *Solid State Comm.*, 82 (1992), 329-34.
- [20] T.B. Massalski, ed., *Binary Alloy Phase Diagram*, Vol. 1. (ASM International, 1990), 203.
- [21] G. Trambly de Laissardière, D. Nguyen Manh, and D. Mayou, “Effective medium-range Mn–Mn pair interaction induces pseudogap in the density of states of Al(Si)–Mn approximants,” *J. Non-Cryst. Solids*, 334-335 (2004), 347-51.
- [22] G. Trambly de Laissardière, and D. Mayou, “Clusters and localisation of electrons in quasicrystals,” *Phys. Rev. B*, 55 (1997), 2890-3.
- [23] G. Trambly de Laissardière, S. Roche, and D. Mayou, “Electronic confinement by clusters in quasicrystals and approximants,” *Mat. Sc. Eng. A*, 226-228 (1997), 986-9.
- [24] S. Ögüt, and K.M. Rabe, “Anomalous effective charges and far-IR optical absorption of Al<sub>2</sub>Ru from first principles,” *Phys. Rev. B*, 54 (1996), R8297.
- [25] D. Nguyen-Manh, A. Bratkovsky, and D.G. Pettifor, “Quantum mechanical predictions in intermetallics modelling,” *Phil. Trans. Royal Soc. Lond. A*, 351 (1995), 529-42.
- [26] D. Nguyen-Manh et al., “Metastability of the  $\omega$ -phase in transition-metal aluminides: first-principles structural predictions,” *Phil. Mag. A*, 74 (1996), 1385-97.

- [27] D. Nguyen-Manh, and D.G. Pettifor, “Electronic structure, phase stability and elastic moduli of AB transition-metal aluminides,” *Intermetallics*, 7 (1999), 1095-106.
- [28] D. Nguyen-Manh, D.G. Pettifor, *Gamma Titanium Alluminides*, ed. Y.W. Kim, (TMS publications, 1999), 175.
- [29] J. Zou, and A.E. Carlsson, “Preferred Mn spacings in Al-Mn compounds,” *Phys. Rev. Lett.*, 70 (1993), 3748-51.
- [30] G. Trambly de Laissardière, and D. Mayou, “Magnetic Properties of Quasicrystals and Approximants,” *Quasicrystals*, Ed. J.B. Suck, M. Schreiber, and P. Häussler, (Berlin: Springer-Verlag, 2002), 487-504.
- [31] V. Simonet et al., “Local order in liquids forming quasicrystals and approximant phases,” *Phys. Rev. B* 65 (2002), 24203(11).
- [32] T. Schenk et al., “Temperature dependence of the chemical short-range order in undercooled and states Al-Fe-Co liquids,” *Europhys. Lett.*, 65 (2004), 34-40.
- [33] A.P. Blandin, *Phase Stability in Metals and Alloys*, Ed. P.S. Rudman, J. Stringer, R.I. Jaffee, (New York: McGraw-Hill, 1967).
- [34] J. Hafner, *From Hamiltonians to Phase Diagrams*, (Berlin: Springer Verlag, 1987).
- [35] K. Robinson, “The Structure of  $\beta$ (AlMnSi)-Mn<sub>3</sub>SiAl<sub>9</sub>,” *Acta Crystallogr.*, 5 (1952), 397.
- [36] C.B. Shoemaker, D.A. Keszler, and D.P. Shoemaker, “Structure of  $\mu$ -MnAl<sub>4</sub> with Composition Close to that of Quasicrystals Phases,” *Acta Crystallogr.*, 45 (1989), 13-20.
- [37] G. Kreiner, and H.F. Franzen, “The crystal structure of  $\lambda$ -Al<sub>4</sub>Mn,” *J. Alloys Compounds*, 261 (1997), 83-104.
- [38] G. Trambly de Laissardière, “Interplay between electronic structure and medium range atomic order in hexagonal  $\beta$ -Al<sub>9</sub>Mn<sub>3</sub>Si and  $\varphi$ -Al<sub>10</sub>Mn<sub>3</sub>,” *Phys. Rev. B*, 68 (2003), 045117(11).
- [39] F. Hippert et al., “Magnetic properties of AlPdMn approximant phases,” *J. Phys.: Condens. Matter*, 11 (1999), 10419-10435.
- [40] F. Hippert et al., “Origin of Magnetism in Al-Pd-Mn and Al-Mn Quasicrystals and Approximants,” *Materials Research Society Symposium Proceedings*, Boston november 2000, Ed. E. Belin-Ferré et al., Vol. 643 (Boston, 2001), K14.2.1-K14.2.12.
- [41] F. Hippert et al., “Localized Magnetism in Molten Icosahedral and Approximant AlPdMn Phases,” *Phys. Rev. Lett.*, 76 (1996), 54-7.
- [42] V. Simonet et al., “Origin of magnetism in crystalline and quasicrystalline AlMn and AlPdMn phases,” *Phys. Rev. B*, 58 (1998), R8865.
- [43] F. Hippert et al., “Magnetic properties of icosahedral Al-Pd-Mn quasicrystals,” *Phys. Rev. B*, 68 (2003), 134402(13).

- [44] C. Berger, “Electronic properties of quasicrystals, experimental,” *Lectures on Quasicrystals*, Ed. F. Hippert, and D. Gratias, (Les Ulis: Les Editions de Physique, 1994), 463-504.
- [45] J.J. Pr ejean, C. Berger, A. Sulpice, and Y. Calvayrac. “Linear increase of the conductivity with the concentration of local defects in AlPdMn quasicrystals,” *Phys. Rev. B*, 65 (2002), R140203(4).
- [46] J. Hafner J, and M. Krajc ı, “Formation of magnetic moments in crystalline, quasicrystalline, and liquid Al–Mn alloys,” *Phys. Rev. B* 57 (1998), 2849-60.
- [47] M. Krajc ı, J. Hafner, “Isolated magnetic moments in icosahedral Al–Pd–Mn alloys,” *Phys. Rev. B*, 58 (1998), 14110-2.
- [48] G. Trambly de Laissardi ere, and D. Mayou, “Magnetism in Al(Si)-Mn Quasicrystals and Related Phases,” *Phys. Rev. Lett.*, 85 (2000), 3273-6.
- [49] A.M. Bratkovsky et al., “Topological disorder as an origin of a magnetic moment on Mn in Al-Mn alloys,” *Phys. Rev. B*, 52 (1995), 3056-9.
- [50] T. Fujiwara, S. Yamamoto S, and G. Trambly de Laissardi ere, “Band structure effects of transport properties in the icosahedral quasicrystals,” *Phys. Rev. Lett.*, 71 (1993), 4166-9.
- [51] G. Trambly de Laissardi ere, and T. Fujiwara, “Electronic structure and conductivity in a model approximant of icosahedral quasicrystal AlCuFe,” *Phys. Rev. B*, 50 (1994), 5999-6005.
- [52] G. Trambly de Laissardi ere, and T. Fujiwara, “Electronic structure and transport in a model Approximant of decagonal quasicrystal AlCuCo,” *Phys. Rev. B*, 50 (1994), 9843-50.
- [53] S. Roche, G. Trambly de Laissardi ere, and D. Mayou, “Electronic transport properties of quasicrystals,” *J. Math. Phys.*, 38 (1997), 1794-1822.
- [54] D. Mayou et al., “Evidence for unconventional electronic transport in quasicrystals” *Phys. Rev. Lett.*, 70 (1993), 3915-8.
- [55] D. Mayou, “Wave propagation in quasiperiodic media,” *Quasicrystals Current Topics* Ed. E. Belin–Ferr e et al., (London: World Scientific, 2000), 412-54.
- [56] D. Mayou, “Generalized Drude Formula for the Optical Conductivity of Quasicrystals,” *Phys. Rev. Lett.*, 85 (2000), 1290-3.
- [57] D.N. Basov et al., “Optical Conductivity of Insulating Al-Based Alloys: Comparison of Quasiperiodic and Periodic Systems,” *Phys. Rev. Lett.*, 73 (1994), 1865-8.
- [58] D. Gratias et al., “Atomic clusters in icosahedral *F*-type quasicrystals,” *Phys. Rev. B*, 63 (2000), 24202(16).
- [59] V. Fourn ee et al., “The electronic structure of orthorhombic Al<sub>2</sub>Ru,” *J. Phys.: Condens. Mater.*, 9 (1997), 7999-8010.

- [60] M. Krajčí, and J. Hafner, “Covalent bonding and bandgap formation in transition-metal aluminides: di-aluminides of group VIII transition metals,” *J. Phys.: Condens. Matter*, 14 (2002), 5755-83; “Covalent bonding and band-gap formation in ternary transition-metal di-aluminides:  $\text{Al}_4\text{MnCo}$  and related compounds,” *J. Phys.: Condens. Matter*, 14 (2002), 7201-19 “Prediction of insulating quasicrystalline approximants using *ab initio* electronic structure calculations,” *Phys. Rev. B*, 67 (1999), 052201(4).
- [61] E.S. Zijlstra, and S.K. Bose, “Detailed *ab initio* electronic structure study of two approximants to Al–Mn based icosahedral quasicrystals,” *Phys. Rev. B*, 67 (2003), 224204(9).